

# Compositional Scene Representation Learning via Reconstruction: A Survey

Jinyang Yuan, Tonglin Chen, Bin Li, and Xiangyang Xue

**Abstract**—Visual scene representation learning is an important research problem in the field of computer vision. The performance of artificial intelligence systems on vision tasks could be improved if more suitable representations are learned for visual scenes. Complex visual scenes are composed of relatively simple visual concepts, and have the property of combinatorial explosion. Compared with directly representing the entire visual scene, extracting compositional scene representations can better cope with the diverse combinations of background and objects. Because compositional scene representations abstract the concept of objects, performing visual scene analysis and understanding based on these representations could be easier and more interpretable. Moreover, learning via reconstruction can greatly reduce the need for training data annotations. Therefore, reconstruction-based compositional scene representation learning has important research significance. In this survey, we first outline the current progress on this research topic, including development history and categorizations of existing methods from the perspectives of modeling of visual scenes and inference of scene representations; then provide benchmarks, including an open source toolbox to reproduce the benchmark experiments, of representative methods that consider the most extensively studied problem setting and form the foundation for other methods; and finally discuss the future directions of this research topic.

**Index Terms**—compositional scene representations, object-based representations, object-centric learning, object-oriented learning, perceptual grouping, image reconstruction.



## 1 INTRODUCTION

VISUAL scene representation learning is an important research problem in the field of computer vision. If more suitable representations can be learned for visual scenes, the performance of artificial intelligence systems on computer vision tasks can be improved [1], [2], [3]. Complex visual scenes are composed of relatively simple visual concepts (objects and backgrounds), and the combination of visual concepts has the property of combinatorial explosion. With only few types of objects, various visual scenes with rich diversity can be created. Therefore, compared with directly representing the entire visual scene, extracting compositional visual scene representations which represent background and each object separately can better cope with the diversity of visual scenes. Because compositional scene representations abstract the concept of objects, performing visual scene analysis and understanding could be easier and more intuitively understood by humans.

Depending on the datasets used in experiments and the naming conventions, compositional scene representation learning is often referred to as perceptual grouping, object-based representation learning, object-centric learning, or object-oriented learning. These terms will be used interchangeably in this survey. The researches on compositional scene representation learning are inspired by humans' ability to perceive visual scenes compositionally. The exploration of this ability is often referred to as the perceptual

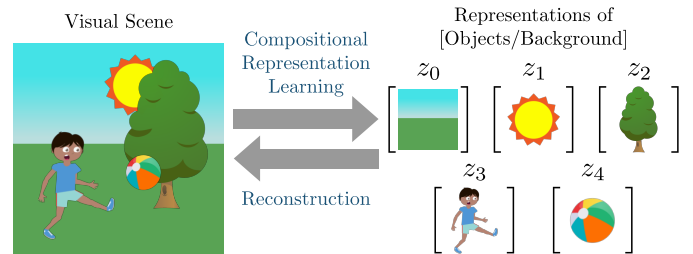


Fig. 1. The general framework of learning compositional scene representations via reconstruction.

grouping problem [4]. Perceptual grouping is a binding problem related to visual perception [5], [6], which mainly studies how the brain groups the basic visual elements (such as pixels) of visual scenes into visual concepts. Representative theories related to perceptual grouping include Gestalt laws of grouping [7], synchronization theory [8], feature integration theory [9]. The Gestalt grouping law summarizes the ways humans perceive visual scenes into several principles, including the principle of proximity, similarity, continuity, closure, and common fate. The common fate principle differs from other principles in that it requires motion information. Synchronization theory assumes that the binding or separation of features of visual concepts is based on the synchronization of neuronal activity in the cerebral cortex. If neurons fire synchronously, then the features corresponding to those neurons are bound, and if neurons fire out of synchronization, then the features corresponding to these neurons are dissociated. Feature integration theory divides visual perception into two stages: in the pre-attentive stage, the brain automatically extracts features of visual scenes

- The authors are with the Shanghai Key Laboratory of Intelligent Information Processing and the School of Computer Science, Fudan University, Shanghai 200433, China.  
E-mail: {yuanjinyang, tchen18, libin, xyxue}@fudan.edu.cn

Manuscript received Month Day, Year; revised Month Day, Year.  
(Corresponding author: Bin Li.)

without attention and awareness; in the focused attention stage, the brain binds the features of each visual concept using the focused attention of the local area, and recognizes the corresponding visual concept if the features are familiar. Among these theories, Gestalt grouping law summarizes the manifestations of perceptual grouping, and synchronization theory and feature integration theory focus on explaining the underlying mechanisms behind perceptual grouping.

Reconstruction is a common way to learn representations for visual scenes. By minimizing reconstruction errors, scene representation methods can learn to extract representations that contain as much information of visual scenes as possible. Because the computation of reconstruction errors does not require additional supervision, learning composition scene representations via reconstruction greatly reduces the need for expensive and laborious manual annotations, and can better exploit massive amounts of unlabeled data.

This survey focuses on the problem of learning compositional scene representations without object-level supervision, by using reconstruction as the main objective. Figure 1 illustrates the general learning framework that consists of two parts, i.e., encoding (compositional scene representation learning) and decoding (reconstruction). This research problem is different from visual scene segmentation, which only requires partitioning scene images and does not necessarily learn scene representations. The considered problem has gained increasing attentions over the past few years, and various methods have been proposed in this direction. Because multiple design choices need to be considered in compositional scene representation learning, the categorization of existing methods is not straightforward. In addition, different methods usually use different sets of datasets and evaluation metrics to conduct experiments, which makes direct comparison of these methods difficult. Therefore, there is a need to systematically categorize and compare existing methods, which motivates the writing of this survey.

This survey is organized as follows: Section 2 provides an overview of reconstruction-based compositional scene representation learning; Sections 3 and 4 categorize existing methods from the perspectives of modeling of visual scenes and inference of scene representations, respectively; Section 5 provides benchmarks of representative methods that consider the most extensively studied problem setting in this research topic<sup>1</sup>; Section 6 looks forward to several directions for future research; Section 7 concludes the whole survey.

## 2 OVERVIEW

In this section, we will first describe the problem setting of reconstruction-based compositional scene representation learning and the notations used in the paper, then introduce the development history of this research topic, and finally give an overview of categorizations of existing methods.

### 2.1 Problem Setting and Notations

In compositional scene representation learning, each visual scene is modeled as the composition of multiple layers of objects and background, and each layer is associated

1. An open source toolbox is provided to reproduce the benchmark experiments. Code is available at <https://tinyurl.com/5bhb6nt3>.

TABLE 1  
Notations used throughout the paper.

Notation	Meaning
$N \in \mathbb{Z}_+$	Number of pixels in each image
$C \in \mathbb{Z}_+$	Number of image channels
$K \in \mathbb{Z}_+$	Number of layers modeling objects
$\mathbf{x} \in \mathbb{R}^{N \times C}$	The observed image
$\tilde{\mathbf{x}} \in \mathbb{R}^{N \times C}$	The reconstructed image
$\mathbf{a}_k \in \mathbb{R}^{N \times C}$	The appearance of the $k$ th layer
$\mathbf{s}_k \in \mathbb{R}^N$	The shape of the $k$ th layer
$\mathbf{z}_k$	The representations of the $k$ th layer

with a series of representations that fully characterize the corresponding object or background. The collection of representations of all the objects and background forms the compositional representations of the visual scene. The problem setting of compositional scene representation learning via reconstruction is to learn separate representations for individual objects and background in the visual scene, by using reconstruction error minimization as the main objective.

The notations used throughout the paper are summarized in Table 1.  $\mathbf{x} \in \mathbb{R}^{N \times C}$  and  $\tilde{\mathbf{x}} \in \mathbb{R}^{N \times C}$  denote the observed and reconstructed images of the visual scene, respectively.  $N$  denotes the number of pixels in each image,  $C$  denotes the number of image channels, and  $K$  denotes the number of layers modeling the objects in the visual scenes. The index of the background layer is 0, and the indexes of the  $K$  object layers are between 1 and  $K$ .  $\mathbf{a}_k \in \mathbb{R}^{N \times C}$  and  $\mathbf{s}_k \in \mathbb{R}^N$  denote the appearance and shape of the  $k$ th layer, respectively.  $\mathbf{z}_k$  denotes the representation of the background ( $k = 0$ ) or the  $k$ th object ( $1 \leq k \leq K$ ).  $f_{\text{bck}}$  and  $f_{\text{obj}}$  are the decoders that transform the representations of background and objects into the corresponding images of layers, respectively, i.e.,  $[\mathbf{a}_k, \mathbf{s}_k] = f_{\text{bck}}(\mathbf{z}_k)$  for  $k = 0$  and  $[\mathbf{a}_k, \mathbf{s}_k] = f_{\text{obj}}(\mathbf{z}_k)$  for  $1 \leq k \leq K$ .  $f_{\text{comp}}$  is the compositing function that transforms all the  $K + 1$  layers into the reconstructed image of visual scene, i.e.,  $\tilde{\mathbf{x}} = f_{\text{comp}}(\mathbf{a}_{0:K}, \mathbf{s}_{0:K})$ .

It is worth mentioning that the number of object layers  $K$  is *not* necessarily equal to the actual number of objects in the visual scene, because different visual scenes may contain different numbers of objects and the actual number of objects in each visual scene is assumed to be *unknown* during learning. In addition, the separate modeling of background with  $\mathbf{z}_0$  and  $f_{\text{bck}}$  is *optional*, and the index of the separately modeled background is chosen to be 0 for notational convenience. Some methods such as RC [10] and N-EM [11] do not consider the background layer, and any object layer contains complete information about the background. Some methods such as IODINE [12] and Slot Attention [13] do not distinguish between background and objects, and the background is modeled identically to objects.

### 2.2 Development History

The development of compositional scene representation learning can be roughly divided into two streams. The first one is mainly inspired by the synchronization theory, and the second one is mainly inspired by the feature integration theory. Representative methods in these two streams are shown in Fig. 2. In the early days of the researches on



### 2.2.2 Methods Mainly Based on Feature Integration Theory

The main idea of the feature integration theory is the application of attention mechanism in visual perception. At the beginning of the research on compositional scene representation learning, methods that are mainly based on the feature integration theory, such as CST-VAE [17] and AIR [18], use bounding boxes of objects as the attention mechanisms, and estimate bounding boxes based on the entire image. Subsequent methods that also use this type of attentions include SuPAIR [23] and ASR [24]. SPAIR [25] combines the main idea of YOLO [46] with compositional scene representation learning, and estimates bounding boxes of objects based on local features. The usage of local features to estimate bounding boxes has inspired various methods, such as SPAIR [25] and SPACE [32], and is one of the current mainstream practices. The other current mainstream practice, which begins with MONet [22] and is adopted by methods like Yang et al. [28] and GENESIS [29], is to use arbitrary-shaped masks to sequentially attend to regions of different objects and background.

During the development of compositional scene representation learning methods that are mainly based on the feature integration theory, some methods adopt the ideas from methods that are mainly inspired by the synchronization theory, and additionally consider the modeling of object motions, relationships among objects, and the problem of learning from multiple viewpoints. For example, GMIOO [21] develops inference method by combining the ideas of using bounding boxes as the attention mechanism and iteratively refining compositional scene representations. GNM [30] models relationships among objects with hierarchical latent variables, and infers latent variables in a way similar to SPACE. SQAIR [20] and ViMON [41] are developed on AIR and MONet, respectively, and additionally considers the modeling of object motions. R-SQAIR [26] integrates SQAIR with graph neural networks [16], [47], and can model the interactions among objects. SILOT [34] and SCALOR [31] extend the idea of SPAIR and SPACE to object tracking, respectively, and can learn composition scene representations from videos. G-SWM [33] considers the modeling of both object relationships and object motions, and can effectively learn from videos with multimodal uncertainty. GSGN [42] uses hierarchical latent variables with tree structure to model visual scenes, and can hierarchically decompose objects into basic components. ROOTS [43] extends the idea of SPAIR to three-dimensional space, and is able to learn compositional scene representations from multiple viewpoints.

### 2.3 Categorizations of Methods

Existing compositional scene representation learning methods can be roughly categorized from two perspectives, i.e., either from the modeling of visual scenes, or from the inference of scene representations. Within each categorization, existing methods can be further subdivided in several aspects. Fig. 3 compares existing methods in these aspects.

#### 2.3.1 Modeling of Visual Scenes

The modeling of visual scenes can be categorized in three major ways. i.e., the composition of layers, the modeling of shapes, and the representation of objects. Moreover, some

Methods	C	S	R	N	L	V	M	I	A
RC [10]	M	N	R-E					RE	A-N
Tagger [14]	M	N	R-E					RE	A-N
RTagger [15]	M	N	R-E				✓	RE	A-N
N-EM [11]	M	N	R-E					EM	A-N
Relational N-EM [16]	M	N	R-E		✓			EM	A-N
LDP [19]	M	S	R-E					EM	A-N
IODINE [12]	M	N	R-L					VI	A-N
MulMON [27]	M	N	R-L			✓		VI	A-N
DyMON [35]	M	N	R-L			✓	✓	VI	A-N
PROVIDE [36]	M	N	R-L				✓	VI	A-N
PSGNet [48]	S	N	R-E				✓	RE	A-F
Slot Attention [13]	S	N	R-E					RE	A-F
EfficientMORL [37]	M/S	N	R-L					VI	A-F
SIMONe [38]	M	N	R-L			✓		VI	A-F
OCLOC [39]	M	O	R-L	✓		✓		VI	A-F
CST-VAE [17]	S	S	R-L					VI	R-G
AIR [18]	S		R-L	✓				VI	R-G
SQAIR [20]	S		R-L	✓			✓	VI	R-G
R-SQAIR [26]	S		R-L	✓	✓		✓	VI	R-G
ASR [24]	S		R-L	✓	✓			VI	R-G
GMIOO [21]	M	S	R-L	✓				VI	R-G
SuPAIR [23]	S	S	R-L	✓				VI	R-G
TBA [49]	S	S	R-E	✓			✓	RE	A-F
SPAIR [25]	S	O	R-L	✓				VI	R-L
SILOT [34]	S	O	R-L	✓			✓	VI	R-L
SPACE [32]	S	O	R-L	✓				VI	R-L
SCALOR [31]	S	O	R-L	✓			✓	VI	R-L
GNM [30]	S	O	R-L	✓				VI	R-L
G-SWM [33]	S	O	R-L	✓	✓		✓	VI	R-L
GSGN [42]	S	O	P-V	✓	✓			VI	R-L
ROOTS [43]	S	O	R-L	✓	✓	✓		VI	R-L
MONet [22]	M	N	R-L					VI	A-N
Yang et al. [28]	M	N	R-L					VI	A-N
ViMON [41]	M	N	R-L				✓	VI	A-N
POD-Net [50]	M	N	R-L				✓	VI	A-N
GENESIS [29]	M	S	R-L		✓			VI	A-N
GENESIS-V2 [40]	M	N	R-L		✓			VI	A-F
DTI-Sprites [51]	S	S	P-I	✓				RE	R-G
PCDNet [52]	S	S	P-I					RE	R-G
MarioNette [53]	S	S	P-V					RE	R-L

Fig. 3. Comparison of compositional scene representation learning methods in terms of: the composition of layers (C); the modeling of shapes (S); the representation of objects (R); whether modeling the number of objects (N), layouts of scenes (L), multi-viewpoints of scenes (V), and motions of objects (M); the inference methods (I); and the attention mechanisms (A). Meanings of the abbreviations in the table are described in the corresponding parts of Sections 3 and 4.

methods consider the modeling of extra properties of visual scenes, e.g., the number of objects, the layouts of scenes, the multi-viewpoint of scenes, and the motions of objects.

**Composition of Layers:** In compositional representation learning methods, a visual scene image is modeled as the composition of foreground objects and background. Layers of background and objects are usually composited in two ways, i.e., either using spatial mixture models or using weighted summations. **1)** Methods using spatial mixture models treat appearances of objects and background as parameters of mixture components, and perceived shapes of objects and background as mixture weights. At each pixel of the visual scene image, the index of the observed layer is first sampled according to mixture weights, and then the color or intensity of the pixel is sampled from the corresponding mixture component. Representative methods

using spatial mixture models include Tagger [14], RC [10], N-EM [11], IODINE [12], MONet [22], GMIOO [21], and GENESIS [29]. **2)** Methods using weighted summations assume that the color or intensity of each pixel is sampled from a unimodal distribution, whose parameters are computed based on the weighted summation of appearances of objects and background. Representative methods using weighted summations include AIR [18], SPAIR [25], SuPAIR [23], SQAIR [20], SPACE [32], and Slot Attention [13].

**Modeling of Shapes:** The perceived shape of objects in the visual scenes are often incomplete due to occlusions, and the modeling of perceived shapes of objects and background is a crucial problem in compositional scene representation learning. **1)** The first way to compute perceived shapes is to directly normalize outputs of neural networks *without* considering complete shapes of objects and background. A commonly used normalization is the softmax function, and representative methods include MONet [22], IODINE [12], and Slot Attention [13]. **2)** The second way is to first compute complete shapes of objects and background, and then use the combination of the softmax function and the stick-breaking process [54] to compute perceived shapes based on both complete shapes and an extra type of variables characterizing the depths of objects. Representative methods include SPAIR [25], SPACE [32], SCALOR [31], and GNM [30]. **3)** The third way also computes perceived shapes by transforming complete shapes with occlusions taken into consideration, and complete shapes are transformed in a way similar to the stick-breaking process. Representative methods include CST-VAE [17], LDP [19], GMIOO [21], and ECON [55]. It is worth mentioning that there are a small number of methods, such as AIR [18] and SQAIR [20], that do not model the perceived shapes, but directly add images of all the layers to obtain the visual scene image.

**Representation of Objects:** Objects in the visual scenes are usually represented in two ways. One way is to use vectors that may take any values in the real vector space as representations of objects, and the other way is to represent objects based on finite number of prototypes. **1)** Methods that represent objects with vectors in the real vector space can be further divided into two categories. The first one is to use latent variables, and the second one is to use embeddings. Representative methods that use latent variables to represent objects include AIR [18], SPAIR [25], IODINE [12], GMIOO [21], MONet [22], GENESIS [29], and EfficientMORL [37], and representative methods that use embeddings to represent objects include Taggers [14], N-EM [11], LDP [19], and Slot Attention [13]. The main difference between latent variables and embeddings is that the former ones are assumed to be sampled from prior distributions in the generative model, while the latter ones do not have prior distributions. **2)** Methods that represent objects based on finite number of prototypes can also be further divided into two categories. The first one is to directly use prototype images that can be transformed into layers of objects with interpretable transformations, and representative methods include DTI-Sprites [51] and PCDNet [52]. The second one is to use prototype vectors that can be transformed into prototype images using neural networks, and representative methods include GSGN [42] and MarioNette [53].

**Additional Modelings:** The above-mentioned aspects

are essential parts of compositional scene representation learning methods. There are other properties, including the **1)** number of object, **2)** layouts of scenes, **3)** multi-viewpoints of scenes, and **4)** motions of objects, that can be additionally modeled to extend the abilities of compositional scene representation learning methods. For example, methods such as AIR [18], GMIOO [21], SPAIR [25], and SPACE [32] model the number of objects, and are able to count objects in the visual scene image by inferring compositional scene representations. Methods such as GENESIS [29], GENESIS-V2 [40], GNM [30] and GSGN [42] model the layouts of scenes. It is worth noting that GNM [30] and GSGN [42] also model the number of objects, and GENESIS-V2 [40] is able to count objects during inference even though the number of objects is not modeled in the modeling of visual scenes. Methods such as MulMON [27], ROOTS [43], DyMON [35], SIMONE [38], and OCLOC [39] model the multi-viewpoints of scenes. Methods such as SQAIR [20], R-SQAIR [26], SILOT [34], SCALOR [31], and G-SWM [33] model both the number and motions of objects, and are able to learn from videos.

### 2.3.2 Inference of Scene Representations

The inference of scene representations can be categorized in two ways, i.e., either from the inference methods, or from the attention mechanisms used during the inference.

**Inference Methods:** The ways to infer compositional scene representations can be divided into three categories. **1)** For methods that use latent variables as representations of objects, e.g., AIR [18], GMIOO [21], IODINE [12], GENESIS [29], and GENESIS-V2 [40], compositional scene representations are inferred based on *amortized variational inference*, and parameters of approximate posterior distributions are estimated with neural networks. **2)** For methods that model visual scenes with spatial mixture models and explicitly infer indicating variables, e.g., N-EM [11], Relational N-EM [16], and LDP [19], the inference is performed in a way inspired by the *Expectation Maximization* algorithm [56]. **3)** For methods that do not use any latent variables in the modeling of visual scene, e.g., RC [10], Tagger [14], RTagger [15], and Slot Attention [13], the inference is learned by minimizing the *reconstruction errors* between the observed and reconstructed images of visual scenes.

**Attention Mechanisms:** In order to learn compositional scene representations, different objects in the same image need to be distinguished. The ways to distinguish objects can all be seen as some types of attention mechanisms, and there are two major ways to design attentions. **1)** One way is to use *rectangular attention*, which first estimates bounding boxes of objects and then extract representations of objects based on the contents in the bounding boxes. Representative methods include AIR [18], SQAIR [20], GMIOO [21], SPAIR [25], and SPACE [32]. **2)** The other way is to use *arbitrary-shaped attention*, which does not restrict the shapes of attentions. Representative methods include N-EM [11], IODINE [12], MONet [22], Slot Attention [13], and GENESIS [29].

## 3 MODELING OF VISUAL SCENES

In this section, we will describe design choices for the modeling of visual scenes in detail, including the composition of layers, the modeling of shapes, the representation of objects, and the modeling of extra properties of visual scenes.

### 3.1 Composition of Layers (C)

The images of visual scenes can be modeled as the composition of layers in two major ways, i.e., either using spatial mixture models or using weighted summations. As shown in Fig. 4, the major difference between these two choices lies in the way of “softness” of occlusions. Methods using spatial mixture models assume that only one layer of object or background is observed at each pixel, and the color or intensity of each pixel is chosen to be the same as the observed layer. Methods using weighted summations assume that objects and background are occluded in a soft way, and the color or intensity of each pixel is the weighted summation of all the layers of objects and background.

#### 3.1.1 Spatial Mixture Models (M)

When using spatial mixture models to composite layers of objects and background, all the pixels of the visual scene image are assumed to be independent of one another. Each pixel  $\mathbf{x}_n$  is associated with a variable  $l_n$  indicating which layer is observed at the pixel. Assuming that the number of layers that model objects in the visual scene is  $K$ , the possible values that  $l_n$  can take is  $\{0, 1, \dots, K\}$ , with  $l_n = 0$  and  $1 \leq l_n \leq K$  indicating that the separately modeled background and the  $l_n$ th object is observed at the  $n$ th pixel, respectively. The joint probability distribution of all the  $N$  pixels in the visual scene image is factorized as

$$p(\mathbf{x}) = \prod_{n=1}^N p(\mathbf{x}_n) = \prod_{n=1}^N \sum_{k=0}^K \underbrace{p(l_n=k)}_{\pi_{k,n}} p(\mathbf{x}_n|l_n=k) \quad (1)$$

In Eq. (1),  $p(l_n)$  is the mixture weight that describes the prior distribution of the indicating variable  $l_n$ , and  $p(\mathbf{x}_n|l_n)$  is the mixture component that describes the conditional distribution of the  $n$ th pixel given that the  $l_n$ th layer of object or background is observed at this pixel. Although pixels are assumed to be independent of one another, spatial dependencies of pixels can still be captured by modeling dependencies of mixture weights  $p(l_n)$ , or parameters of mixture components  $p(\mathbf{x}_n|l_n)$ , or both of them with neural networks. In spatial mixture models, mixture weights  $p(l_n)$  can be interpreted as the perceived shapes of objects and background (may be incomplete due to occlusions), and are usually modeled by categorical distributions. As for mixture components  $p(\mathbf{x}_n|l_n)$ , they are parameterized by appearances of objects and background, and are usually chosen to be Bernoulli distributions for binary images and normal distributions for grayscale or color images, respectively. For all the methods that use spatial mixture models to composite layers of objects and background, parameters of mixture components  $p(\mathbf{x}_n|l_n)$  are computed by transforming representations of objects and background with neural networks. As for mixture weights  $p(l_n)$ , the computation can be classified into the following three categories.

In methods like RC [10] and N-EM [11], all the mixture components correspond to objects, and the regularization used in the learning of compositional scene representations encourages all the components also contain complete information of background. Because the background of visual scene image is not modeled by a specific mixture component, the 0th layer which corresponds to separately

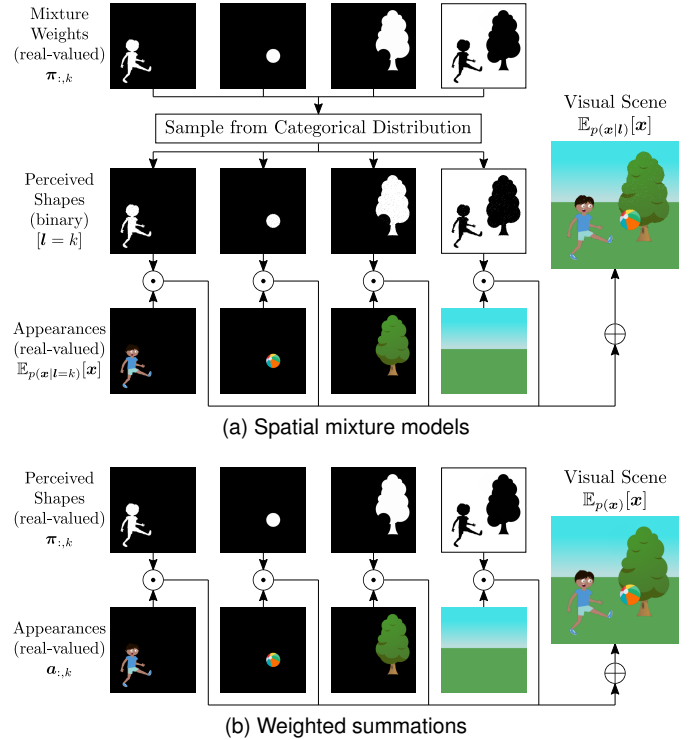


Fig. 4. Comparison of different types of layer composition.

modeled background for notational convenience is not used in these methods. Mixture weights are usually assumed to be spatially independent, and the values of  $p(l_n = k)$  are set to 0 if  $k = 0$  and set to  $1/K$  if  $1 \leq k \leq K$  for all the pixels.

In methods like IODINE [12] and MONet [22], the modelings of objects and background are identical. Therefore, it is not straightforward to identify the background component that is not separately modeled, and the 0th layer which is specifically assigned to separately modeled background is absent in these methods. For the 0th layer, mixture weights  $p(l_n = 0)$  are set to 0 for all the pixels. For the  $k$ th layer with  $1 \leq k \leq K$ , mixture weights  $p(l_n = k)$  are computed by transforming representations of objects and background with a neural network.

In methods like LDP [19] and GMIOO [21], objects and background are distinguished in the modeling of visual scenes. Mixture weights of objects ( $1 \leq k \leq K$ ) are computed based on a neural network that takes the representation of each object as input, and mixture weights of background ( $k = 0$ ) are assumed to be complementary to the sum of mixture weights of all the objects, i.e.,  $p(l_n = 0) = 1 - \sum_{k=1}^K p(l_n = k)$  for all the pixels.

#### 3.1.2 Weighted Summations (S)

Same as methods that composite layers of objects and background using spatial mixture models, methods using weighted summations also assume the independence among all the pixels of the visual scene image, i.e.,  $p(\mathbf{x}) = \prod_{n=1}^N p(\mathbf{x}_n)$ . The main difference between these two types of methods is that the latter ones do not model the distribution of each pixel  $p(\mathbf{x}_n)$  with a mixture model, but instead model  $p(\mathbf{x}_n)$  with a unimodal distribution such as Bernoulli distribution (for binary images) or normal distribution (for

grayscale or color images). The expected value of each pixel  $\mathbf{x}_n$  is used as the parameter of the distribution  $p(\mathbf{x}_n)$ , and is modeled as a weighted summation of appearances of all the objects and background using the following expression.

$$\mathbb{E}_{\mathbf{x}_n \sim p(\mathbf{x}_n)}[\mathbf{x}_n] = \sum_{k=0}^K \pi_{k,n} \mathbf{a}_{k,n} \quad (2)$$

In Eq. (2),  $\pi_{k,n}$  and  $\mathbf{a}_{k,n}$  are the weight and appearance of the  $k$ th layer of object or background at the  $n$ th pixel, respectively. Despite the assumption of independence of all the pixels, the weights  $\pi$ , or the appearances  $\mathbf{a}$ , or both of them can be assumed to be spatially dependent in order to model the spatial relationships of pixels. According to the constraints on the weights  $\pi$ , methods using weighted summations to composite different layers of objects and background can be classified into two categories.

In methods like AIR [18] and SQAIR [20], the only constraint placed on the weights  $\pi$  is that the values of weights should all be either 0 or 1, i.e.,  $\pi_{k,n} \in \{0, 1\}$  for all the pixels and layers. The weights of the 0th layer that models the background of the visual scene image are all assumed to be 1, i.e.,  $\pi_{n,0} = 1$  for all the pixels. The weights of the  $k$ th layer with  $1 \leq k \leq K$  are determined by the bounding box of the  $k$ th object in the visual scene image, i.e.,  $\pi_{k,n} = 1$  for every pixel inside or on the  $k$ th bounding box, and  $\pi_{k,n} = 0$  for every pixel outside the  $k$ th bounding box. Because the weights of all the layers may not sum up to 1 at each pixel, this kind of weighted summation does not have an interpretable physical meaning.

In methods like CST-VAE [17] and SPAIR [25], besides the constraint that the weights should all be in the range  $[0, 1]$ , the sum of weights of all the layers is constrained to be 1 at every pixel, i.e.,  $\sum_{k=0}^K \pi_{k,n} = 1$  for all the  $1 \leq n \leq N$ . In this kind of weighted summation, the weights  $\pi$  can be interpreted as the perceived shapes of objects and background, and the computation of Eq. (2) may be interpreted as an  $\alpha$ -weighted convex combination of objects and background, which is widely adopted in the rendering of images in the field of computer graphics.

### 3.2 Modeling of Shapes (S)

With the exception of very few methods such as AIR [18] and SQAIR [20], which composite layers into visual scene images using weighted summations that do not constrain the weights to sum up to 1 at each pixel, the mixture weights in methods using spatial mixture models to composite layers and the weights in methods using weighted summations to composite layers may both be interpreted as the perceived shapes of objects and background (may be incomplete due to occlusions). As shown in Fig. 5, existing methods can be classified into three categories according to the modeling of perceived shapes, i.e., directly normalizing outputs of neural networks with the softmax function, or first computing complete shapes and depth ordering of objects and then normalizing these variables, or first computing complete shapes and then transforming complete shapes in a way similar to the stick-breaking process. The first one has the advantage of requiring simpler computations, while the second and the third ones have the advantage of being able

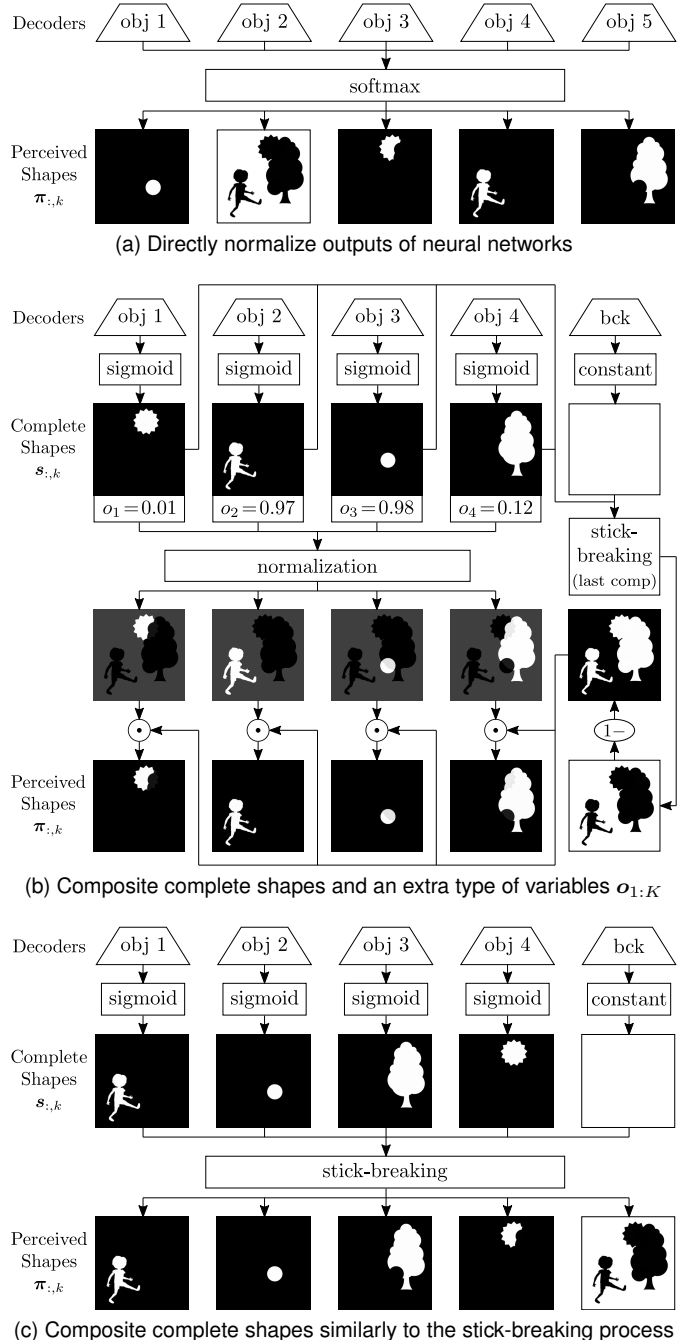


Fig. 5. Comparison of different types of shape modeling.

to additionally determine the complete shapes and depth ordering of objects based on the inference results.

#### 3.2.1 Normalization of Network Outputs (N)

In methods like MONet [22], IODINE [12], and Slot Attention [13], perceived shapes are modeled by directly normalizing outputs of neural networks, and objects and background are usually not distinguished in the modeling of visual scenes. Therefore, the indexes of the layers that model either objects or background are both between 1 and  $K$ , and the perceived shape of the 0th layer is 0 at all the pixels. The representation of each object or background  $z_k$  is transformed into a real-valued variable  $s_k$  that contains the shape information of the  $k$ th layer with a neural network,

and the range of the value that each entry  $s_{k,n}$  can take is not constrained. For all the pixels, the mixture weights of the spatial mixture models or the weights used in the weighted summations  $\pi_n$  are computed using the softmax function.

$$\pi_{k,n} = \begin{cases} 0, & k = 0 \\ \frac{\exp(s_{k,n})}{\sum_{k'=1}^K \exp(s_{k',n})}, & 1 \leq k \leq K \end{cases} \quad (3)$$

### 3.2.2 Normalization of Complete Shapes and Ordering (O)

In methods like SPAIR [25], SPACE [32], SCALOR [31], and GNM [30], outputs of neural networks are first transformed into complete shapes  $s_{0:K}$  and a type of variables  $o_{1:K}$  indicating the depth ordering of objects, and then normalized into perceived shapes. For all the objects, the value of  $o_k$  is constrained to be greater than 0, and can be achieved by functions like the sigmoid function or the exponential function. Objects with larger  $o_k$  are assumed to occlude those with smaller  $o_{k'}$ , and the background is assumed to be occluded by all the objects. The ascending depth ordering or objects can be obtained by sorting variables  $o_k$  in descending order. Perceived shapes  $\pi_{0:K}$  are computed using the following expression.

$$\pi_{k,n} = \begin{cases} \prod_{k'=1}^K (1 - s_{k',n}), & k = 0 \\ (1 - \pi_{n,0}) \frac{s_{k,n} o_k}{\sum_{k'=1}^K s_{k',n} o_{k'}}, & 1 \leq k \leq K \end{cases} \quad (4)$$

### 3.2.3 Stick-Breaking Composition of Complete Shapes (S)

In methods like CST-VAE [17], LDP [19], GMIOO [21], and ECON [55], perceived shapes are modeled in a way similar to the stick-breaking process. Objects with smaller indexes are assumed to occlude objects with larger indexes, and the background is occluded by all the objects. The ascending depth ordering of objects is identical to the object index ordering. Complete shapes  $s_{0:K}$  are transformed into perceived shapes  $\pi_{0:K}$  using the following expression.

$$\pi_{k,n} = \begin{cases} \prod_{k'=1}^K (1 - s_{k',n}), & k = 0 \\ s_{k,n} \prod_{k'=1}^{k-1} (1 - s_{k',n}), & 1 \leq k \leq K \end{cases} \quad (5)$$

## 3.3 Representation of Objects (R)

The main goal of compositional scene representation learning is to learn separate representation for each object or background in the visual scene image. Based on the possible values that representations can take, existing methods can be classified into two categories, i.e., either using representations in the real vector space, or represent objects based on finite number of prototypes. Methods in the former category have the advantage of requiring simpler inference and training strategy, and methods in the latter category are advantageous in that they have an additional ability to distinguish different types of objects.

### 3.3.1 Representations in Real Vector Space (R)

In methods that use vectors in the real vector space to represent objects, representations are first transformed into layers of objects with neural networks, and then composited

to form the visual scene image based on either spatial mixture models or weighted summations. Depending whether defining the prior distributions of representations, existing methods can be divided into the following two categories.

**Embeddings (E):** In methods like N-EM [11] and Slot Attention [13], objects are represented in the form of embeddings, and no prior distribution is placed on the representations. These methods only define the conditional generative model of visual scenes, and do not provide a natural way to generate images when no image is provided after training.

**Latent Variables (L):** In methods like AIR [18] and IODINE [12], objects are represented in the form of latent variables. These methods define the complete generative model of visual scenes, and assume latent variables to be sampled from prior distributions. A commonly used prior distribution is the standard normal distribution  $\mathcal{N}(\mathbf{0}, \mathbf{I})$ . Based on the sampled latent variables, visual scene images that are similar to those used for training can be generated.

### 3.3.2 Finite Number of Prototypes (P)

In methods that represent objects based on finite number of prototypes, a dictionary of prototypes is used in the modeling of visual scenes, and is shared in the generation of all the visual scene images. Each visual scene image is generated by first transforming prototypes into layers based on the identity variables that are either sampled from prior distributions or manually given, and then compositing all the layers using either spatial mixture models or weighted summations. According to the forms of prototypes, existing methods can be divided into two categories, i.e., either using images or using low-dimensional vectors as prototypes. The main difference between these two categories is that the methods in the second category use an extra step to transform prototype vectors into prototype images.

**Images (I):** In methods like DTI-Sprites [51] and PCDNet [52], each type of object is associated with a prototype image. To generate layers of objects in visual scenes, parameterized transformations that are well interpretable, e.g., geometric transformations and colorimetric transformations, are applied to prototype images. The prototype images are randomly initialized at the beginning of the training, and automatically learned from data as training progresses.

**Vectors (V):** In methods like GSGN [42] and MarioNette [53], prototype images are further represented by low-dimensional vectors, and an additional neural network is used to decode prototype vectors. The generated prototype images are transformed into layers that composite scene images in a way similar to DTI-Sprites and PCDNet. To learn the dictionary of prototype vectors, all the entries in the dictionary are first randomly initialized and then iteratively updated based on the inference results of training data.

## 3.4 Additional Modelings

Besides the above-mentioned essential parts in the modeling of visual scenes, there are other properties of visual scenes that can be additionally considered to extend the abilities of compositional scene representation learning methods. For example, modeling the number of objects in the visual scenes provides a natural way to count objects by inference, modeling layouts of visual scenes enables the learned models to generate visual scene images with more reasonable

layouts and thus improves the usefulness of the generated images, modeling multi-viewpoints of visual scenes enables learning from extra viewpoints that provide additional information of the visual scenes, and modeling motions of objects enables learning dynamics of objects from videos and predicting the changes of visual scenes in the future.

### 3.4.1 Number of Objects ( $N$ )

The number of objects in the visual scene image is usually modeled as the sum of binary variables  $z_{1:\infty}^{\text{pres}}$  or  $z_{1:I,1:J}^{\text{pres}}$  that indicate the presences of objects in the visual scene. According to the modeling of these binary variables, existing methods can be divided into three categories.

In methods like AIR [18] and SQAIR [20], each visual scene is assumed to contain possibly infinite number of objects. Each object is associated with a binary variable  $z_k^{\text{pres}}$  that equals 1 if this object appears in the visual scene and equals 0 otherwise. The generative process of  $z_{1:\infty}^{\text{pres}}$  and the computation of the number of objects  $\tilde{K}$  are

$$z_k^{\text{cond}} \sim \text{Bernoulli}(\alpha), \quad k \geq 1 \quad (6)$$

$$z_k^{\text{pres}} = \prod_{k'=1}^k z_{k'}^{\text{cond}}, \quad k \geq 1 \quad (7)$$

$$\tilde{K} = \sum_{k=1}^{\infty} z_k^{\text{pres}} \quad (8)$$

In the above expressions,  $\alpha$  is a hyperparameter that controls the prior distribution of the number of objects, which is in the form of a geometric distribution. Intermediate variables  $z_{1:\infty}^{\text{cond}}$  are first sampled from Bernoulli distributions parameterized by  $\alpha$ , and then transformed to variables  $z_{1:\infty}^{\text{pres}}$ . The computation of variables  $z_{1:\infty}^{\text{pres}}$  ensures that the starting  $\tilde{K}$  entries  $z_{1:\tilde{K}}^{\text{pres}}$  are all 1, and the following entries  $z_{\tilde{K}+1:\infty}^{\text{pres}}$  are all 0, i.e.,  $z_{1:\infty}^{\text{pres}}$  can be seen as the unary code for the number of objects  $\tilde{K}$ .

In methods like SPAIR [25] and SPACE [32], each visual scene image is partitioned into  $I \times J$  regions, and each region at the  $i$ th row and  $j$ th column is associated with a binary variable  $z_{i,j}^{\text{pres}}$  indicating whether there is an object centered in this region. In another word, each region is assumed to contain zero or one object whose center is in the region, and the maximum possible number of objects in the visual scene is  $I \times J$ . The number of objects is modeled using the following expressions.

$$z_{i,j}^{\text{pres}} \sim \text{Bernoulli}(\alpha), \quad 1 \leq i \leq I, 1 \leq j \leq J \quad (9)$$

$$\tilde{K} = \sum_{i=1}^I \sum_{j=1}^J z_{i,j}^{\text{pres}} \quad (10)$$

Different from methods like AIR [18] and SQAIR [20], all the variables  $z_{i,j}^{\text{pres}}$  are independent of one another, which lowers the difficulty of inference. It should be noted that it is straightforward to model visual scene images containing more than  $I \times J$  objects, by either increasing the values of  $I$  and  $J$ , or assuming that there may be multiple objects centered in each region and sampling multiple binary variables  $z_{i,j,1:K_{\max}}^{\text{pres}}$  for each region.

Similar to methods like AIR [18] and SQAIR [20], methods like GMIOO [21] also assume that there may be infinite number of objects in each visual scene, and assign a binary variable  $z_k^{\text{pres}}$  to each object to indicate its presence in the visual scene. The main difference between these two types of methods is that methods like GMIOO break the direct

dependencies among  $z_{1:\infty}^{\text{pres}}$  assigned to different objects by independently sampling  $z_k^{\text{pres}}$  from Bernoulli distributions whose parameters have dependencies. The generative modeling of the number of objects is described below.

$$\nu_k \sim \text{Beta}(\alpha, 1), \quad k \geq 1 \quad (11)$$

$$z_k^{\text{pres}} \sim \text{Bernoulli}(\prod_{k'=1}^k \nu_{k'}), \quad k \geq 1 \quad (12)$$

$$\tilde{K} = \sum_{k=1}^{\infty} z_k^{\text{pres}} \quad (13)$$

The binary variables  $z_{1:\infty}^{\text{pres}}$  sampled using the above expressions can be seen as a single-row infinite-column binary matrix that is sampled using the Indian Buffet Process (IBP) [57], [58]. The dependencies among parameters of the Bernoulli distributions used to sample variables  $z_{1:\infty}^{\text{pres}}$  encourage  $z_k^{\text{pres}}$  with larger index  $k$  more likely to be 0. The introduction of latent variables  $\nu$  breaks the direct dependencies among  $z_k^{\text{pres}}$  with different  $k$ , and makes the inference of variables  $z_{1:\infty}^{\text{pres}}$  easier at the cost of additionally inferring latent variables  $\nu$ .

### 3.4.2 Layouts of Scenes ( $L$ )

The layouts of visual scenes can be modeled by considering the relationships among objects in the modeling of visual scenes. A common way to model the relationships among objects is to model the dependencies among representations of objects. According to the ways the dependencies are modeled, existing methods can be classified in three categories.

In methods like GENESIS [29] and GENESIS-V2 [40], dependencies among representations of objects are modeled by factorizing the joint probability distribution  $p(z_{1:K})$  using the chain rule and modeling the conditional distributions using a recurrent neural network (RNN). The factorization of the joint probability distribution is

$$p(z_{1:K}) = \prod_{k=1}^K p(z_k | z_{1:k-1}) = \prod_{k=1}^K p(z_k | \mathbf{h}_k) \quad (14)$$

In the above expressions,  $\mathbf{h}_k = f_{\text{RNN}}(z_{k-1}, \mathbf{h}_{k-1})$  is the hidden states of the RNN  $f_{\text{RNN}}$  at the  $k$ th step, and is recurrently updated using  $f_{\text{RNN}}$  based on both the hidden states of the previous step  $\mathbf{h}_{k-1}$  and the representation of the previous object  $z_{k-1}$ . The hidden states of the first object  $\mathbf{h}_1$  are randomly initialized, and the hidden states  $\mathbf{h}_k$  with  $k > 1$  summarize the information contained in the representations of objects whose indexes are less than  $k$ . For all the objects, the hidden states  $\mathbf{h}_k$  are transformed into parameters of the conditional distribution  $p(z_k | z_{1:k-1})$  using the same neural networks.

In methods like GNM [30], each visual scene image is partitioned into  $I \times J$  regions, and each region at the  $i$ th row and  $j$ th column is associated with a set of latent variables  $z_{i,j}$  that characterize this region. The layout of the visual scene is described by an extra latent variable  $z^{\text{lyt}}$ , and the joint probability distribution of  $z^{\text{lyt}}$  and latent variables of all the regions  $z_{1:I,1:J}$  is factorized as

$$p(z^{\text{lyt}}, z_{1:I,1:J}) = p(z^{\text{lyt}}) \prod_{i=1}^I \prod_{j=1}^J p(z_{i,j} | z^{\text{lyt}}) \quad (15)$$

Latent variables  $z_{i,j}$  of different regions are conditionally independent of one another given the layout latent variable  $z^{\text{lyt}}$ , and in general have dependencies when  $z^{\text{lyt}}$  is

unknown. Although latent variables  $z_{i,j}$  with different  $i$  and  $j$  are independently sampled from the corresponding conditional distribution  $p(z_{i,j}|z^{\text{lyt}})$ , there can still be spatial relationships among these latent variables by using a neural network, e.g., the StructDRAW adopted by GNM [30], to transform the layout latent variable  $z^{\text{lyt}}$  into parameters of all the conditional distributions.

In methods like GSGN [42], the layout of each visual scene is assumed to be hierarchical and is represented in the form of a tree. The leaf nodes of the tree represent primitive entities of the visual scene, e.g., simple objects or basic components of relatively complex objects, and edges of the tree represent transformations applied to lower-level entities to compose higher-level entities. Let  $\mathcal{V}$  denote the set of all the nodes in the tree, and  $z_v$  represent the representations of node  $v$ . The joint probability of the representations of all the nodes is factorized according to the structure of the tree.

$$p(z_{\mathcal{V}}) = \prod_{v \in \mathcal{V}} p(z_v | pa(z_v)) \quad (16)$$

In the above expression,  $pa(z_v)$  denotes the parent node of node  $v$ . This factorization exploits the fact that a node in a tree is conditionally independent of other nodes given its parent node. The prior distribution of the root node can be chosen to be a predefined distribution, e.g., a standard normal distribution  $\mathcal{N}(\mathbf{0}, \mathbf{I})$ , and the conditional distributions of other nodes are modeled using the same neural networks.

### 3.4.3 Multi-Viewpoints of Scenes ( $V$ )

For visual scenes that may be observed from multiple viewpoints, the modeling of visual scenes needs to additionally consider viewpoints in order to learn viewpoint-independent representations of individual objects and background. In compositional scene representation learning methods that consider the modeling of  $M$  multiple viewpoints, the representations of each visual scene are divided into two parts. The first part  $z_{1:M}^{\text{view}}$  characterizes the  $M$  viewpoints to observe the visual scene, and the second part  $z_{0:K}^{\text{attr}}$  contains information of the viewpoint-independent attributes of objects and background. For each viewpoint, layers  $[\mathbf{a}_{m,0:K}, \mathbf{s}_{m,0:K}]$  of objects ( $1 \leq k \leq K$ ) and background ( $k=0$ ) are computed using the following expressions.

$$[\mathbf{a}_{m,k}, \mathbf{s}_{m,k}] = \begin{cases} f_{\text{bck}}(z_m^{\text{view}}, z_k^{\text{attr}}), & k=0 \\ f_{\text{obj}}(z_m^{\text{view}}, z_k^{\text{attr}}), & 1 \leq k \leq K \end{cases} \quad (17)$$

In Eq. (17),  $f_{\text{bck}}$  and  $f_{\text{obj}}$  are neural networks that take both  $z_m^{\text{view}}$  and  $z_k^{\text{attr}}$  as inputs, and generate layers of background and objects, respectively. Different neural networks are used for background and objects for generality. By distinguishing between viewpoints and viewpoint-independent representations, a well-trained reconstruction-based compositional scene representation learning method is able to synthesize images of the same visual scene from multiple novel viewpoints by keeping viewpoint-independent representations  $z_{1:K}^{\text{attr}}$  unchanged and only modifying the variable  $z_m^{\text{view}}$  that characterizes viewpoint. According to the forms of the variables  $z_{1:M}^{\text{view}}$ , existing methods can be divided into the following two categories.

In methods like MulMON [27], DyMON [35], and ROOTS [43], the exact viewpoints to observe each visual

scene are assumed to be known, and the annotations of viewpoints are used as  $z_{1:M}^{\text{view}}$  in both the training of the model and the inference of compositional scene representations after training. Compositional scene representation learning methods in this category are expected to extract viewpoint-independent representations given viewpoint annotations, and have the advantage of being able to synthesize images observed from specific viewpoints. The major challenge for these methods is to include as many viewpoint-independent attributes and as little viewpoint information as possible in the learned representations. A common practice is to extract scene representations using images observed from some viewpoints, and encourage the learned representations to be able to predict images observed from other viewpoints as accurate as possible.

Methods like SIMONE [38] and OCLOC [39] consider a harder problem of learning compositional scene representations from multiple viewpoints without knowing viewpoints, and learn representations for both viewpoints and viewpoint-independent attributes of objects and background. The major challenge for these methods is to automatically disentangle viewpoints and viewpoint-independent attributes in situations where there may be infinite possible solutions (e.g., due to the change of global coordinate system of the visual scene). Compared with compositional scene representation learning methods that utilize viewpoint annotations, methods in this category have the advantage of being applicable to completely unlabeled data. Among methods that learn from multiple viewpoints without viewpoint annotations, some methods like SIMONE [38] assume that the viewpoints used to observe each visual scene are ordered, while other methods like OCLOC [39] assume that the viewpoints are unordered. Methods assuming ordered viewpoints can better utilize the temporal information to guide the learning of compositional scene representations, while methods assuming unordered viewpoints do not require relationships among viewpoints, and can thus be applied to a wider range of scenarios.

### 3.4.4 Motions of Objects ( $M$ )

Videos of visual scenes contain rich temporal information that can be utilized to improve the learning of compositional scene representations. In order to better learn from videos, motions of objects need to be modeled because they are the main causes of temporal changes of video frames. Methods that consider motions of objects in the modeling of visual scenes usually divide objects in each frame into two parts. The first part consists of objects that have been seen in the previous frames, and the second part consists of objects that newly appear in the current frame. The modeling of objects in the first part is usually termed as *propagation*, which aims to capture dynamics of objects by conditioning the representations of objects in the current frame on the representations of previous frames. The modeling of objects in the second part is usually termed as *discovery*, which aims to capture the prior distribution of representations of objects that enter the visual scene for the first time. Let  $z_{t,k}$  denote the representation of the  $k$ th object in the  $t$ th frame, and  $\tilde{K}_t$  denote the total number of distinct objects that have been seen in the first  $t$  frames. The index of the same object is identical in all the frames. Depending on the choices of

specific methods, the same object that disappears from the visual scene and then reappears may be treated as either one or two distinct objects. The joint probability distribution of representations of all the  $\tilde{K}_T$  objects that have been seen in  $T$  frames is factorized in the way described below.

$$p(\mathbf{z}) = \prod_{t=1}^T \underbrace{p^{\text{P}}(\mathbf{z}_{t,1:\tilde{K}_{t-1}} | \mathbf{z}_{1:t-1,1:\tilde{K}_{t-1}})}_{\text{propagation}} \underbrace{p^{\text{D}}(\mathbf{z}_{t,\tilde{K}_{t-1}+1:\tilde{K}_t})}_{\text{discovery}} \quad (18)$$

In Eq. (18),  $p^{\text{P}}(\mathbf{z}_{t,1:\tilde{K}_{t-1}} | \mathbf{z}_{1:t-1,1:\tilde{K}_{t-1}})$  is the conditional probability distribution of the representations of objects that have been seen at least once between frame 1 and frame  $t-1$ . The representations  $\mathbf{z}_{t,1:\tilde{K}_{t-1}}$  in the  $t$ th frame depend on the representations  $\mathbf{z}_{1:t-1,1:\tilde{K}_{t-1}}$  in all the previous frames.  $p^{\text{D}}(\mathbf{z}_{t,\tilde{K}_{t-1}+1:\tilde{K}_t})$  is the prior distribution of all the objects that have not been seen between frame 1 and frame  $t-1$ . The number of the objects in the 0th frame  $\tilde{K}_0$  is set to be 0. Objects in the discovery part are usually modeled to be independent of one another for simplicity, i.e., the discovery can be factorized as  $p^{\text{D}}(\mathbf{z}_{t,\tilde{K}_{t-1}+1:\tilde{K}_t}) = \prod_{k=\tilde{K}_{t-1}+1}^{\tilde{K}_t} p(\mathbf{z}_{t,k})$  for all the frames. According to whether considering the relationships among objects in the modeling of the propagation part  $p^{\text{P}}(\mathbf{z}_{t,1:\tilde{K}_{t-1}} | \mathbf{z}_{1:t-1,1:\tilde{K}_{t-1}})$ , existing methods can be divided into the following two categories.

In methods like SQAIR [20] and SILOT [34], relationships among objects are not considered in the modeling of the propagation part, and the motion of each object is independently modeled. The propagation part is factorized as

$$p^{\text{P}}(\mathbf{z}_{t,1:\tilde{K}_{t-1}} | \mathbf{z}_{1:t-1,1:\tilde{K}_{t-1}}) = \prod_{k=1}^{\tilde{K}_{t-1}} p^{\text{P}}(\mathbf{z}_{t,k} | \mathbf{z}_{1:t-1,k}) \quad (19)$$

One usual practice used in the modeling of  $p^{\text{P}}(\mathbf{z}_{t,k} | \mathbf{z}_{1:t-1,k})$  is to use a recurrent neural network (RNN) to summarize the information of representations  $\mathbf{z}_{1:t-1,k}$  from frame 1 to frame  $t-1$  in the hidden states  $\mathbf{h}_k^t$  in a way similar to Eq. (14). In this way, the same neural network can be applied to the hidden states  $\mathbf{h}_k^t$  of the RNN to compute parameters of the distributions  $p^{\text{P}}(\mathbf{z}_{t,k} | \mathbf{z}_{1:t-1,k})$  for all the frames.

In methods like R-SQAIR [26] and G-SWM [33], interactions among objects are considered in the modeling of object motions, and the propagation part captures the relationships of objects. In order to model relationships among a variable number of objects while maintaining the computational cost relatively low, representations of all the objects in the same frame are usually assumed to be conditionally independent of one another given the representations in all the previous frames. The propagation part is factorized as

$$p^{\text{P}}(\mathbf{z}_{t,1:\tilde{K}_{t-1}} | \mathbf{z}_{1:t-1,1:\tilde{K}_{t-1}}) = \prod_{k=1}^{\tilde{K}_{t-1}} p^{\text{P}}(\mathbf{z}_{t,k} | \mathbf{z}_{1:t-1,1:\tilde{K}_{t-1}}) \quad (20)$$

The conditional distribution  $p^{\text{P}}(\mathbf{z}_{t,k} | \mathbf{z}_{1:t-1,1:\tilde{K}_{t-1}})$  can be modeled using the combination of a recurrent neural network (RNN) and a graph neural network (GNN). The hidden states  $\mathbf{h}_k^t$  assigned to each object summarize relevant information from representations of all the objects in all the previous frames  $\mathbf{z}_{1:t-1,1:\tilde{K}_{t-1}}$ , and are recurrently updated by an RNN. The inputs to the RNN are the previous hidden states  $\mathbf{h}_k^{t-1}$  and a variable  $e_{t-1,k}$  that is transformed

from  $\mathbf{z}_{t-1,1:\tilde{K}_{t-1}}$  with a GNN modeling interactions among objects. To compute parameters of  $p^{\text{P}}(\mathbf{z}_{t,k} | \mathbf{z}_{1:t-1,1:\tilde{K}_{t-1}})$ , a neural network shared across all the frames and objects is applied to transform the hidden states  $\mathbf{h}_k^t$ .

## 4 INFERENCE OF SCENE REPRESENTATIONS

The inference of scene representations is the inverse process of the modeling of visual scenes, and aims to extract compositional scene representations that can be used to reconstruct the observed visual scenes well. There are two main aspects that need to be considered in the inference. The first one is the choice of inference method, and the second one is the attention mechanism used in the inference.

### 4.1 Inference Methods (I)

There are mainly three types of commonly used inference methods, namely, the amortized variational inference, the Expectation Maximization (EM) algorithm, and the direct optimization of reconstruction error. The type of the inference method used by a compositional scene representation learning method is usually determined by the modeling of visual scenes, and some details of the inference method, such as the inference networks and attention mechanisms, may be chosen independently of the specific modeling of visual scenes. The amortized variational inference is commonly used by methods that represent visual scenes in the form of latent variables. The EM algorithm is commonly adopted by methods that do not use latent variables as compositional scenes representations, but use some latent variables, e.g., the indicator variables of spatial mixture models, in the modeling of visual scenes. Methods that do not use any type of latent variables usually directly optimize reconstruction errors of visual scene images to learn the inference of compositional scene representations.

#### 4.1.1 Amortized Variational Inference (VI)

For methods that represent visual scenes in the form of latent variables  $\mathbf{z}$  and define prior distribution of  $\mathbf{z}$  in the generative modeling of visual scenes, e.g., CST-VAE [17], AIR [18], SQAIR [20], IODINE [12], and MONet [22], the goal of the inference is to estimate the posterior distribution  $p(\mathbf{z} | \mathbf{x})$  of latent variables  $\mathbf{z}$  given the observed visual scene image  $\mathbf{x}$ . By using the Bayes rule, the posterior distribution  $p(\mathbf{z} | \mathbf{x})$  can be computed using the prior distribution  $p(\mathbf{z})$  and the likelihood function  $p(\mathbf{x} | \mathbf{z})$  that have already been defined in the modeling of visual scenes, i.e.,  $p(\mathbf{z} | \mathbf{x}) = \frac{p(\mathbf{x} | \mathbf{z})p(\mathbf{z})}{\int p(\mathbf{x} | \mathbf{z})p(\mathbf{z})d\mathbf{z}}$ . The integral  $\int p(\mathbf{x} | \mathbf{z})p(\mathbf{z})d\mathbf{z}$  appearing in the denominator, however, is in general intractable. One viable solution that is commonly used in compositional scene representation learning is to perform variational inference that approximates the intractable posterior distribution  $p(\mathbf{z} | \mathbf{x})$  with the variational distribution  $q(\mathbf{z} | \mathbf{x})$  that is tractable to estimate. The goal of variational inference is to find parameters of  $q(\mathbf{z} | \mathbf{x})$  that maximize the following expression.

$$\mathcal{L}_{\text{elbo}} = \mathbb{E}_{q(\mathbf{z} | \mathbf{x})} [\log p(\mathbf{x} | \mathbf{z})] - D_{\text{KL}}(q(\mathbf{z} | \mathbf{x}) || p(\mathbf{z})) \quad (21)$$

It can be shown that Eq. (21) is the lower bound of log-evidence  $\log p(\mathbf{x})$ , and is thus usually referred to as evidence lower bound (ELBO). On the right-hand side of Eq. (21),

$\mathbb{E}_{q(\mathbf{z}|\mathbf{x})}[\log p(\mathbf{x}|\mathbf{z})]$  is the reconstruction term that encourages latent variables  $\mathbf{z}$  sampled from the variational distribution  $q(\mathbf{z}|\mathbf{x})$  to be able to reconstruct the observed visual scene image  $\mathbf{x}$  as well as possible, and  $D_{\text{KL}}(q(\mathbf{z}|\mathbf{x})||p(\mathbf{z}))$  is the Kullback-Leibler (KL) divergence term that regularizes the inferred representations by encouraging the aggregated posteriors  $\mathbb{E}_{p_{\text{data}}(\mathbf{x})}[q(\mathbf{z}|\mathbf{x})]$  of the representations of all the training images sampled from  $p_{\text{data}}(\mathbf{x})$  to be close to the prior distribution  $p(\mathbf{z})$ . The detailed expression to compute the KL divergence of two distributions  $q$  and  $p$  is  $D_{\text{KL}}(q||p) = \mathbb{E}_q[\log q - \log p]$ . In order to reduce the computations in the inference and improve the inference speed, compositional scene representation learning methods usually adopt amortized variational inference that uses an inference neural network to transform the observed visual scene image  $\mathbf{x}$  into parameters of the variational distribution  $q(\mathbf{z}|\mathbf{x})$ . It is also possible to apply iterative amortized inference [59] to improve the estimation of parameters of  $q(\mathbf{z}|\mathbf{x})$  by iteratively updating the parameters based on the value of ELBO described in Eq. (21).

Learning model parameters by directly maximizing the ELBO expressed in Eq. (21) may result in over-emphasis on the reconstruction term  $\mathbb{E}_{q(\mathbf{z}|\mathbf{x})}[\log p(\mathbf{x}|\mathbf{z})]$ . The difference between the aggregated posteriors  $\mathbb{E}_{p_{\text{data}}(\mathbf{x})}[q(\mathbf{z}|\mathbf{x})]$  and the prior distribution  $p(\mathbf{z})$  of latent variables may be relatively large, and the quality of sampled images may not be satisfying. To alleviate this problem, Methods like GENESIS [29] and GENESIS-V2 [40] use generalized ELBO with constrained optimization (GECO) [60] as the learning objective. In GECO, the learning objective is to minimize the KL divergence  $D_{\text{KL}}(q(\mathbf{z}|\mathbf{x})||p(\mathbf{z}))$  under the constraint that the reconstruction term is greater than or equal to a constant  $C$ , i.e.,  $\mathbb{E}_{q(\mathbf{z}|\mathbf{x})}[\log p(\mathbf{x}|\mathbf{z})] \geq C$ . The optimization of the GECO objective can be solved using Lagrange multipliers.

#### 4.1.2 Expectation Maximization (EM)

Methods that do not use latent variables as compositional representations of visual scenes but use some latent variables in the modeling of visual scenes usually design inference methods based on the Expectation Maximization (EM) algorithm. The indicator variables used in spatial mixture models, i.e., the variable  $l_n$  in Eq. (1), is a representative type of such latent variables. In spatial mixture models that do not represent visual scenes in the form of latent variables, compositional representations  $\mathbf{z}$  can be seen as parameters of the probability distribution of visual scene images  $\mathbf{x}$ , i.e.,  $p(\mathbf{x}; \mathbf{z}) = \prod_{n=1}^N p(\mathbf{x}_n; \mathbf{z})$ . Due to the multimodality of the distribution  $p(\mathbf{x}_n; \mathbf{z}) = \sum_{k=0}^K p(l_n = k; \mathbf{z})p(\mathbf{x}_n|l_n = k; \mathbf{z})$ , it is hard to infer representations  $\mathbf{z}$  by directly maximizing the log-probability  $\log p(\mathbf{x}; \mathbf{z})$ . A commonly used solution is to iteratively maximize the Q-function  $\mathcal{Q}(\mathbf{z}, \mathbf{z}^{\text{old}})$ , which is computed using the following expression.

$$\mathcal{Q}(\mathbf{z}, \mathbf{z}^{\text{old}}) = \sum_{n=1}^N \sum_{k=0}^K \underbrace{p(l_n = k|\mathbf{x}; \mathbf{z}^{\text{old}})}_{\gamma_{k,n}} \log p(\mathbf{x}_n, l_n; \mathbf{z}) \quad (22)$$

In Eq. (22),  $\gamma_{k,n} = p(l_n = k|\mathbf{x}; \mathbf{z}^{\text{old}})$  is the posterior probability of the indicator variable  $l_n$ , and can be computed using the Bayes rule. The computation of this term only depends on the previous estimation of the representations  $\mathbf{z}^{\text{old}}$  and

the data  $\mathbf{x}$ , and need not be optimized. It can be shown that the value of log-probability  $\log p(\mathbf{x}; \mathbf{z})$  increases as the value of Q-function  $\mathcal{Q}(\mathbf{z}, \mathbf{z}^{\text{old}})$  increases. The optimization of Eq. (22) consists of two alternating steps, i.e. the expectation step (E-step) and the maximization step (M-step). The E-step estimates the posteriors  $\gamma_{0:K}$ , and the M-step finds the representations  $\mathbf{z}$  that maximizes the Q-function described in Eq. (22). Due to the non-linearities of the neural networks used to transform the representations  $\mathbf{z}$  into parameters of the distribution  $p(\mathbf{x}_n, l_n; \mathbf{z})$ , it is in general intractable to find the optimal  $\mathbf{z}$  in the M-step. N-EM [11] provides a solution that uses neural networks to update  $\mathbf{z}$  based on the value of Q-function in the M-step, and methods like Relational N-EM [16] and LDP [19] perform inference under the similar framework. Although the value of Q-function is not guaranteed to increase in each M-step, empirical results have verified the effectiveness of this solution.

#### 4.1.3 Reconstruction Error (RE)

Methods that do not use any latent variables in the modeling of visual scenes, e.g., RC [10], Tagger [14], RTagger [15], and Slot Attention [13], usually use an encoder neural network to directly transform the observed image  $\mathbf{x}$  into the corresponding compositional scene representations  $\mathbf{z}$ , and the objective of the learning is to minimize the reconstruction error, i.e., the difference between the observed image  $\mathbf{x}$  and the reconstructed image  $\tilde{\mathbf{x}}$ . To compute the reconstructed image  $\tilde{\mathbf{x}}$ , these methods first infer compositional representations  $\mathbf{z}_{0:K}$ , then transform  $\mathbf{z}_{0:K}$  into perceived shapes  $\boldsymbol{\pi}_{0:K}$  and appearances  $\mathbf{a}_{0:K}$  according to the modeling of visual scenes, and finally compute the color or intensity of each pixel by  $\tilde{\mathbf{x}}_n = \sum_{k=0}^K \pi_{k,n} \mathbf{a}_{k,n}$ . A commonly used metric to measure the reconstruction error is the mean squared error, and the objective of the learning in this case becomes the minimization of the following expression.

$$\mathcal{L} = \frac{1}{N} \sum_{n=1}^N \|\tilde{\mathbf{x}}_n - \mathbf{x}_n\|_2^2 \quad (23)$$

The minimization of Eq. (23) also has a probabilistic interpretation. By treating compositional representations  $\mathbf{z}$  as parameters of the probability  $p(\mathbf{x}; \mathbf{z})$  and assuming that each pixel  $\mathbf{x}_n$  is independently distributed according to a normal distribution with  $\tilde{\mathbf{x}}_n$  as the mean vector and  $\sigma_x \mathbf{I}$  as the constant covariance matrix, minimizing Eq. (23) is equivalent to maximizing the log-probability  $\log p(\mathbf{x}; \mathbf{z})$ .

## 4.2 Attention Mechanisms (A)

In order to distinguish different objects and background in the visual scene, almost all the compositional scene representation learning methods use attention mechanisms to focus on different regions of visual scenes and guide the inference of representations. Based on the type of attention mechanisms, existing methods can be roughly divided into two categories. Methods in the first type estimate bounding boxes of objects, and use features of the rectangular regions defined by bounding boxes to extract representations of objects. Methods in the second type estimate attention masks that are not restricted to be rectangular. Rectangular and arbitrary-shaped attention masks have their own advantages. The former one is easier to estimate, and the latter

one can better suppress information contained in irrelevant regions if attention masks are correctly estimated.

#### 4.2.1 Rectangular Attention (R)

Methods that adopt rectangular attentions usually represent visual scene images in the form of latent variables, and explicitly model parameters of bounding boxes of objects with latent variables  $z_{1:K}^{\text{bbox}}$  or  $z_{1:I,1:J}^{\text{bbox}}$ . For each object, the latent variable  $z_k^{\text{bbox}}$  or  $z_{i,j}^{\text{bbox}}$  is first inferred, and then the local region of visual scene image in the bounding box parameterized by  $z_k^{\text{bbox}}$  or  $z_{i,j}^{\text{bbox}}$  is cropped and used to estimate the latent variable  $z_k^{\text{attr}}$  or  $z_{i,j}^{\text{attr}}$  that characterizes intrinsic attributes of the object such as shape and appearance in the canonical coordinate. Existing methods can be further divided into two categories based on the features used to estimate bounding boxes of objects. Methods of one type use features of the entire visual scenes to estimate bounding boxes, while methods of the other type divide visual scenes into multiple local regions and estimate bounding boxes centered in local regions based on local features. The main ideas of these two types of attentions are shown in Fig. 6.

**Global Features (G):** In methods like CST-VAE [17] and AIR [18], the latent variables  $z_k^{\text{bbox}}$  and  $z_k^{\text{attr}}$  of each object are inferred alternately, and the variational distribution of latent variables  $z_{1:K}^{\text{bbox}}$  and  $z_{1:K}^{\text{attr}}$  of all the  $K$  object layers is factorized according to the following expression.

$$q(z^{\text{bbox}}, z^{\text{attr}}) = \prod_{k=1}^K q(z_k^{\text{bbox}} | z_{1:k-1}^{\text{bbox}}, z_{1:k-1}^{\text{attr}}) q(z_k^{\text{attr}} | z_k^{\text{bbox}}) \quad (24)$$

The latent variable  $z_k^{\text{bbox}}$  that parameterizes the bounding box of the  $k$ th object is assumed to be dependent on the latent variables  $z_{1:k-1}^{\text{bbox}}$  and  $z_{1:k-1}^{\text{attr}}$  of all the previously inferred objects, and the latent variable  $z_k^{\text{attr}}$  that characterizes intrinsic attributes of the  $k$ th object is assumed to be conditionally independent of latent variables of other objects given  $z_k^{\text{bbox}}$ . For each object, parameters of the conditional distribution  $q(z_k^{\text{bbox}} | z_{1:k-1}^{\text{bbox}}, z_{1:k-1}^{\text{attr}})$  can be estimated either based on the global features of an image that is initialized as the observed image  $x$  and iteratively updated using latent variables  $z_{1:k-1}^{\text{bbox}}$  and  $z_{1:k-1}^{\text{attr}}$ , or based on the hidden states of an RNN that iteratively integrated the global features of the observed image  $x$  with latent variables  $z_{1:k-1}^{\text{bbox}}$  and  $z_{1:k-1}^{\text{attr}}$ .

**Local Features (L):** In methods like SPAIR [25] and SPACE [32], each visual scene image is divided into  $I \times J$  regions, and the inference of both latent variables  $z_{1:I,1:J}^{\text{bbox}}$  and  $z_{1:I,1:J}^{\text{attr}}$  is based on local features of these regions. Different from methods using global features to estimate bounding boxes, methods using local features first infer latent variables  $z_{1:I,1:J}^{\text{bbox}}$  that parameterize bounding boxes of objects for all the local regions, and then infer latent variables  $z_{1:I,1:J}^{\text{attr}}$  that characterize intrinsic attributes of objects. Let  $[(i_1, j_1), (i_2, j_2), \dots, (i_{I \times J}, j_{I \times J})]$  denote the predefined sequence of indexes of  $I \times J$  regions, and  $\mathcal{S}_k$  denote a subset of  $\{1, 2, \dots, k-1\}$ . The factorization of the variational distribution of latent variables  $z_{1:I,1:J}^{\text{bbox}}$  and  $z_{1:I,1:J}^{\text{attr}}$  of all the  $I \times J$  regions is described below.

$$q(z^{\text{bbox}}, z^{\text{attr}}) = \prod_{k=1}^{I \times J} q(z_{i_k, j_k}^{\text{bbox}} | z_{(i,j)_{\mathcal{S}_k}}^{\text{bbox}}) q(z_{i_k, j_k}^{\text{attr}} | z_{i_k, j_k}^{\text{bbox}}) \quad (25)$$

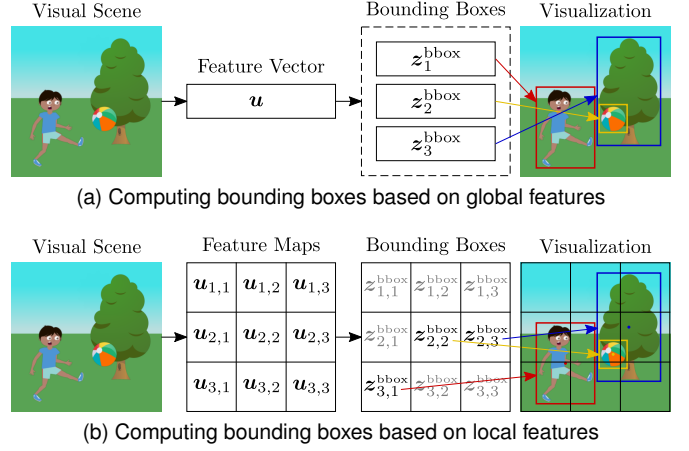


Fig. 6. Two types of rectangular attentions.

In the above expression, parameters of the conditional distribution  $q(z_{i_k, j_k}^{\text{bbox}} | z_{(i,j)_{\mathcal{S}_k}}^{\text{bbox}})$  are estimated based on features of local regions. In methods like SPAIR [25],  $\mathcal{S}_k = \{1, 2, \dots, k-1\} \cap \{k' : (i_{k'}, j_{k'}) \text{ is a neighbor of } (i_k, j_k)\}$ . The inference of  $z_{i_k, j_k}^{\text{bbox}}$  uses local features of the region  $(i_k, j_k)$  and its nearby regions that have already been inferred, and each  $z_{i_k, j_k}^{\text{bbox}}$  is inferred sequentially. In methods like SPACE [32],  $\mathcal{S}_k = \emptyset$ . The inference of  $z_{i_k, j_k}^{\text{bbox}}$  only uses local features of the region  $(i_k, j_k)$ , and each  $z_{i_k, j_k}^{\text{bbox}}$  is inferred in parallel. After estimating bounding boxes of all the regions, parameters of the conditional distribution  $q(z_{i_k, j_k}^{\text{attr}} | z_{i_k, j_k}^{\text{bbox}})$  are simultaneously estimated for all the regions. It is worth mentioning that in order to deal with the situation that some regions may not contain objects whose centers are within the regions, methods using local features usually model the number of objects in the visual scene by assigning a binary latent variable  $z_{i,j}^{\text{pres}}$  indicating the presence of object to each region. Compared with methods using global features, methods using local features restrict the search space of bounding boxes and can better model the spatial invariance of objects. Therefore, these methods can better learn from images with high resolutions.

#### 4.2.2 Arbitrary-Shaped Attention (A)

Methods that use arbitrary-shaped attentions can be further classified into two categories based on the computation of attention masks. Methods of one type compute attention masks based on outputs of decoder networks, while methods of the other type compute attention masks based on similarities of local features extracted by encoder networks. The main ideas of these two types are shown in Fig. 7.

**Network Outputs (N):** In methods like MONet [22], Yang et al. [28], ViMON [41], and POD-Net [50], the perceived shapes of objects and background are first estimated using the combination of an encoder network and a decoder network like U-Net [61], and then the representation of each object or background is inferred based on the concatenation of the estimated perceived shape and the observed image. In methods like GENESIS [29], the representation of each object or background is divided into two parts that characterize the shape attribute and appearance attribute, respectively. After inferring representations that characterize the shape attributes in an autoregressive manner, the decoded perceived

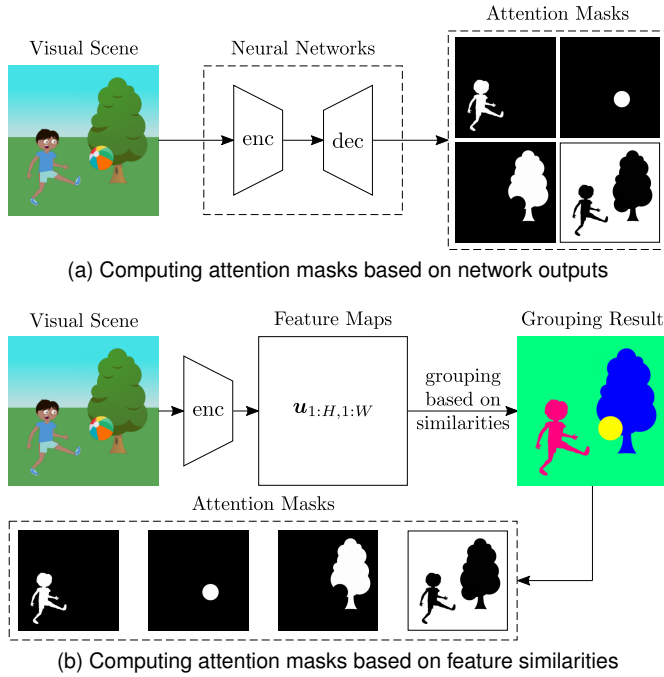


Fig. 7. Two types of arbitrary-shaped attentions.

shapes are concatenated with the observed image and used as attention masks to help the inference of representations that characterize the appearance attributes. In methods like IODINE [12], representations of different objects and background are randomly initialized and iteratively updated. The perceived shapes computed based on the representations inferred in the previous step are used as one of the auxiliary inputs and act as attention masks in the inference of representations in the current step. In methods like N-EM [11] and LDP [19], which iteratively infer compositional representations based on the EM algorithm, the posteriors  $\gamma_{k,n} = p(l_n = k | \mathbf{x}; \mathbf{z}^{\text{old}})$  in Eq. (22) can be seen as attention masks of different layers.

**Feature Similarities (F):** In methods like TBA [49], Slot Attention [13], and EfficientMORL [37], each object is associated with a hidden state of RNN or a vector call slot that characterizes the representation of object. The hidden states or slots are first randomly initialized and then iteratively updated based on the feature maps of the visual scene and the attention masks. The feature maps are extracted using an encoder network, and the attention masks are computed based on the similarity among local features in the feature maps and hidden states or slots. In methods like GENESIS-V2 [40], attention masks are computed in a way inspired by instance coloring, which has been previously used in supervised instance segmentation. The attention mask of each object is sequentially computed based on similarities among all the local features in the feature maps and the local feature at a randomly sampled position. The probability of sampling the position depends on the attention masks of all the processed objects. In methods like PSGNet [48], a convolutional neural network (CNN) with long-range feedback connections is used to extract feature maps of the visual scene at different levels, and label propagation is used to recursively group different regions from finer levels to coarser levels. The grouping results are used as attention

maps to compute features of the grouped regions.

## 5 BENCHMARKS

Compositional scene representation learning is still in the early stages of research, and different methods usually use different sets of datasets and evaluation metrics to conduct experiments, either because of the lack of consensus benchmarks, or because these methods are proposed for different problem settings. This section aims to benchmark the inference performance of representative methods that learn compositional representations of static visual scenes from a single viewpoint. This problem setting is the most extensively studied one, and forms the foundation for more complex problem settings that take object interactions, object motions<sup>2</sup>, or multiple viewpoints into consideration. We reimplement or unify the I/O interfaces of 10 representative methods that are either the state of the arts or usually chosen to be the compared methods in this problem setting, and make the code for creating datasets and evaluating the performance of the chosen methods publicly available. In the following, we first introduce the datasets used to benchmark these methods, then describe the evaluation metrics, and finally compare the performance on different datasets.

### 5.1 Datasets

Four datasets are used to evaluate the performance of different methods. These datasets are constructed based on the MNIST [62], dSprites [63], CLEVR [64], and SHOP VRB [65] datasets<sup>3</sup>, and are referred to as the *MNIST*, *dSprites*, *CLEVR*, *SHOP* datasets for simplicity. The first three datasets are representative datasets that are widely adopted by existing methods, while the last one is a new dataset with more realistic synthesized visual scenes for compositional scene representation learning. These datasets are constructed similarly to the Multi-Objects dataset [66], and additionally provide annotations of complete shapes of different methods so that it possible to assess the performance of different methods with more evaluation metrics. The configurations used to construct these datasets are described in Table 2. In images of the MNIST and dSprites datasets, colors of objects and background are all uniformly sampled in the RGB space  $[0, 1]^3$ , with the constraint that the  $l_2$  distance between the colors of background and any object is at least 0.5. The images of the CLEVR and SHOP datasets are generated based on the official code. The original images rendered by the 3D engine are  $214 \times 160$ , and are cropped into  $128 \times 128$  by removing 19, 67, 43, and 43 pixels from the top, bottom, left, and right sides, respectively. In order to make sure that each object is still visible in the cropped image, the official code is modified and the visibility of objects are checked based on the cropped image. Samples of images in these datasets are shown in Fig. 8.

### 5.2 Metrics

Six metrics are used to quantitatively assess the performance of different methods from four aspects, i.e., segmentation,

2. For benchmarks of representative methods that learn from dynamic visual scenes, please refer to Weis et al. [41] for more details.

3. We manually select 10 objects and 1 background from the SHOP VRB dataset because some objects and backgrounds are too complex for the current compositional scene representation learning methods.

TABLE 2  
Configurations of the MNIST, dSprites, CLEVR, and SHOP datasets.

Datasets	MNIST				dSprites				CLEVR / SHOP			
Splits	Train	Valid	Test 1	Test 2	Train	Valid	Test 1	Test 2	Train	Valid	Test 1	Test 2
# of Images	50000	1000	1000	1000	50000	1000	1000	1000	50000	1000	1000	1000
# of Objects	2 ~ 4	2 ~ 4	2 ~ 4	5 ~ 6	2 ~ 5	2 ~ 5	2 ~ 5	6 ~ 8	3 ~ 6	3 ~ 6	3 ~ 6	7 ~ 10
Image Size	64 × 64				64 × 64				128 × 128			
Min Visible	25%				25%				128 pixels			

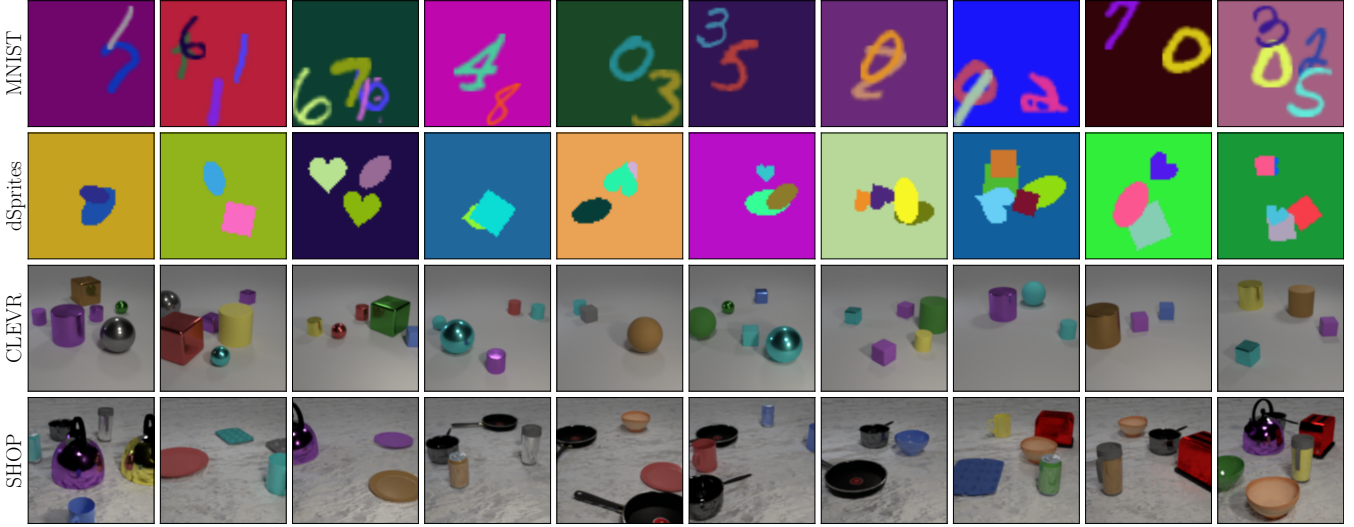


Fig. 8. Samples of images in the MNIST, dSprites, CLEVR, and SHOP datasets.

amodal segmentation, object counting, and object ordering. Segmentation is the most general aspect where all the methods can be evaluated. The remaining three aspects have more requirements on the inference results, and are not applicable to all the methods.

### 5.2.1 Segmentation

The quality of image segmentation measures how accurately the image is decomposed into different objects and background, and is evaluated using Adjusted Mutual Information (AMI) [67] and Adjusted Rand Index (ARI) [68]. AMI and ARI are the two most basic metrics, and almost all the compositional scene representation learning methods are evaluated using one or both of them. Two variants of AMI and ARI are used in order to evaluate the segmentation performance more thoroughly. AMI-A and ARI-A are computed using pixels in the entire image, and measure how accurately different layers of objects and background are separated. AMI-O and ARI-O are computed only using pixels in the regions of objects, and focus on how accurately different objects are separated from one another.

Let  $I$  denote the number of test images. For each test image,  $\hat{K}_i$  denotes the actual number of objects in the image, and  $\hat{\rho}^i \in \{0, 1, \dots, \hat{K}_i\}^N$  and  $\rho^i \in \{0, 1, \dots, K\}^N$  denote the actual and estimated pixel-wise partitions of the image, respectively.  $\hat{r}^i \in \{0, 1\}^{(\hat{K}_i+1) \times N}$  and  $r^i \in \{0, 1\}^{(K+1) \times N}$  are the respective one-hot representations of partitions  $\hat{\rho}^i$  and  $\rho^i$ .  $\mathcal{D}$  denotes the set of pixel indexes used to compute AMI and ARI, i.e.,  $\mathcal{D} = \{1, 2, \dots, N\}$  when computing AMI-A

and ARI-A, and  $\mathcal{D} = \{n : x_n \text{ is in regions of objects}\}$  when computing AMI-O and ARI-O. The computations of AMI and ARI are described below.

$$\text{AMI} = \frac{1}{I} \sum_{i=1}^I \frac{\text{MI}(\hat{\rho}_{\mathcal{D}}^i, \rho_{\mathcal{D}}^i) - \mathbb{E}[\text{MI}(\hat{\rho}_{\mathcal{D}}^i, \rho_{\mathcal{D}}^i)]}{(\text{H}(\hat{\rho}_{\mathcal{D}}^i) + \text{H}(\rho_{\mathcal{D}}^i))/2 - \mathbb{E}[\text{MI}(\hat{\rho}_{\mathcal{D}}^i, \rho_{\mathcal{D}}^i)]} \quad (26)$$

$$\text{ARI} = \frac{1}{I} \sum_{i=1}^I \frac{b_{\text{all}}^i - b_{\text{row}}^i \cdot b_{\text{col}}^i / c^i}{(b_{\text{row}}^i + b_{\text{col}}^i)/2 - b_{\text{row}}^i \cdot b_{\text{col}}^i / c^i} \quad (27)$$

In Eq. (26), MI and H denote mutual information and entropy, respectively. In Eq. (27),  $b_{\text{all}}^i$ ,  $b_{\text{row}}^i$ ,  $b_{\text{col}}^i$ , and  $c^i$  are intermediate variables. Let  $C(x, y)$  denote the number of combinations  $\frac{x!}{(x-y)! y!}$ , and  $v_{k,k}^i$  denote the dot product  $\sum_{n \in \mathcal{D}} (\hat{r}_{k,n}^i \cdot r_{k,n}^i)$ . The computations of these intermediate variables are described below.

$$b_{\text{all}}^i = \sum_{k=0}^{\hat{K}_i} \sum_{k=0}^K C(v_{k,k}^i, 2) \quad (28)$$

$$b_{\text{row}}^i = \sum_{k=0}^{\hat{K}_i} C\left(\sum_{k=0}^K v_{k,k}^i, 2\right) \quad (29)$$

$$b_{\text{col}}^i = \sum_{k=0}^K C\left(\sum_{k=0}^{\hat{K}_i} v_{k,k}^i, 2\right) \quad (30)$$

$$c^i = C\left(\sum_{k=0}^{\hat{K}_i} \sum_{n \in \mathcal{D}} \hat{r}_{k,n}^i, 2\right) \quad (31)$$

### 5.2.2 Amodal Segmentation

The performance of amodal segmentation measures how accurately the complete shapes of objects are estimated, and provides additional information compared to the segmentation performance because the quality of object shape

estimations in occluded regions are considered. Intersection over Union (IoU) and  $F_1$  score (F1) are used to evaluate the performance of amodal segmentation. The former one tends to reflect the worst performance of complete shape estimations among all the objects in the image, while the latter one tends to reflect the average performance. These metrics are only evaluated for methods that are able to estimate complete shapes of objects.

Let  $\hat{s}_{1:\hat{K}_i}^i \in [0, 1]^{\hat{K}_i \times N}$  and  $s_{1:K}^i \in [0, 1]^{K \times N}$  denote the actual and estimate complete shapes of objects in the  $i$ th test image, respectively. In order to compute IoU and F1, the correspondences between layers in the actual and estimated complete shapes need to be determined, because  $\hat{K}_i$  and  $K$  may not be equal, and the orderings of objects may be different in  $\hat{s}_{1:\hat{K}_i}^i$  and  $s_{1:K}^i$ .  $\Xi$  denotes the set containing all the  $K!$  possible permutations of the indexes  $\{1, 2, \dots, K\}$ . The correspondences between  $\hat{s}_{1:\hat{K}_i}^i$  and  $s_{1:K}^i$  are computed by  $\xi^i = \arg \max_{\xi \in \Xi} \sum_{k=1}^{\hat{K}_i} \sum_{n=1}^N \hat{r}_{k,n}^i \cdot r_{\xi_k^i, n}^i$ , which can be efficiently solved based on linear sum assignment. IoU and F1 are computed using the following expressions.

$$\text{IoU} = \frac{1}{I} \sum_{i=1}^I \frac{1}{\hat{K}_i} \sum_{k=1}^{\hat{K}_i} \frac{\sum_{n=1}^N \min(\hat{s}_{k,n}^i, s_{\xi_k^i, n}^i)}{\sum_{n=1}^N \max(\hat{s}_{k,n}^i, s_{\xi_k^i, n}^i)} \quad (32)$$

$$\text{F1} = \frac{1}{I} \sum_{i=1}^I \frac{1}{\hat{K}_i} \sum_{k=1}^{\hat{K}_i} \frac{2 \cdot \sum_{n=1}^N \min(\hat{s}_{k,n}^i, s_{\xi_k^i, n}^i)}{\sum_{n=1}^N \hat{s}_{k,n}^i + \sum_{n=1}^N s_{\xi_k^i, n}^i} \quad (33)$$

### 5.2.3 Object Counting

For methods that additionally model the number of objects in the visual scene image, Object Counting Accuracy (OCA) is used to measure the performance of object number estimation. OCA is computed by dividing the number of images in which the numbers of objects are correctly estimated by the total number of images.

Let  $\hat{K}_i$  and  $\tilde{K}_i$  be the actual and estimated numbers of objects in the  $i$ th test image, respectively, and  $\delta$  denote the Kronecker delta function. The computation of OCA is

$$\text{OCA} = \frac{1}{I} \sum_{i=1}^I \delta_{\hat{K}_i, \tilde{K}_i} \quad (34)$$

### 5.2.4 Object Ordering

Object Ordering Accuracy (OOA) is used to evaluate the accuracy of depth ordering estimation for methods that additionally model the depth ordering of objects. The computation of OOA is based on the weighted average of pairwise ordering estimations of objects. The weight of each pair of objects is the overlapping area determined by the complete shapes of these objects. Different pairs of objects do not use the same weights because the ordering of two objects with a higher degree of overlap can be more easily estimated.

Similar to the evaluation of amodal segmentation performance, the evaluation of object ordering performance also requires computing correspondences between objects in the annotations and estimated results. Let  $\xi^i = \arg \max_{\xi \in \Xi} \sum_{k=1}^{\hat{K}_i} \sum_{n=1}^N \hat{r}_{k,n}^i \cdot r_{\xi_k^i, n}^i$  denote the correspondences computed in the way described in the amodal segmentation part, and  $\hat{\eta}_{k_1, k_2}^i \in \{0, 1\}$  and  $\eta_{\xi_{k_1}^i, \xi_{k_2}^i}^i \in \{0, 1\}$  denote the actual and estimated pairwise orderings of the

$k_1$ th and  $k_2$ th objects in the  $i$ th test image, respectively.  $\hat{\eta}_{k_1, k_2}^i$  and  $\eta_{\xi_{k_1}^i, \xi_{k_2}^i}^i$  equal 1 if the depth of the  $k_1$ th object is smaller than the  $k_2$ th object and equal 0 otherwise. The overlapping area of the  $k_1$ th and  $k_2$ th objects is computed based on the actual complete shapes of objects  $\hat{s}$ , i.e.,  $w_{k_1, k_2}^i = \sum_{n=1}^N \hat{s}_{k_1, n}^i \cdot \hat{s}_{k_2, n}^i$ , and OOA is computed using the following expression.

$$\text{OOA} = \frac{1}{I} \sum_{i=1}^I \frac{\sum_{k_1=1}^{\hat{K}_i-1} \sum_{k_2=k_1+1}^{\hat{K}_i} w_{k_1, k_2}^i \cdot \delta_{\hat{\eta}_{k_1, k_2}^i, \eta_{\xi_{k_1}^i, \xi_{k_2}^i}^i}}{\sum_{k_1=1}^{\hat{K}_i-1} \sum_{k_2=k_1+1}^{\hat{K}_i} w_{k_1, k_2}^i} \quad (35)$$

## 5.3 Performance

The performance evaluated on the Test1 and Test 2 splits of different datasets are shown in Tables 3 and 4, respectively. Because AIR [18] does not model the shapes of objects, and N-EM [11], IODINE [12], MONet [22], Slot Attention [13], EfficientMORL [37], and GENESIS-V2 [40] directly normalize the outputs of neural networks into perceived shapes and cannot estimate complete shapes of objects, the IoU and F1 scores are not evaluated for these methods. Because N-EM [11], IODINE [12], Slot Attention [13], and EfficientMORL [37] randomly initialize and iteratively update representations of objects in parallel, there is no natural ordering of the inferred objects and the OOA scores are not evaluated for these methods. Although N-EM [11], IODINE [12], MONet [22], GENESIS [29], Slot Attention [13], EfficientMORL [37], and GENESIS-V2 [40] do not consider the number of objects in the modeling of visual scenes, objects can still be counted heuristically based on the segmentation results, i.e., the estimated number of objects is considered to be the number of segments for N-EM [11] because the background is not modeled in this method, and is considered to be the number of segments minus one for the other methods that model the background. Based on the results in Tables 3 and 4, the following findings are observed:

- On datasets that are constructed based on layer compositions, i.e., the MNIST and dSprites datasets, GMIOO [21] performs best in almost all the settings. The possible reason is that GMIOO not only models visual scenes in a way similar to the synthesis of images in these datasets, but also adopts an iterative inference method that is beneficial for handling occlusions of objects.
- On datasets where images are rendered using 3D engines, i.e., the CLEVR and SHOP datasets, MONet [22] achieves the best scores in most settings, possibly because it applies U-Net to estimate arbitrary-shaped attention masks based on hierarchical features, which can help distinguish different objects and background more precisely and benefit the learning of compositional scene representations.
- For all the methods, the performance in general does not degrade much when test images contain more objects than those used for training, which has verified the generalizability of compositional scene representation learning.

## 6 FUTURE DIRECTIONS

Future studies of compositional scene representation learning via reconstruction can be carried out from two aspects. One aspect is the learning of compositional scene representations. For example, combining compositional scene

TABLE 3  
Comparison of different compositional scene representation learning methods on the Test 1 splits.

Dataset	Method	AMI-A	ARI-A	AMI-O	ARI-O	IoU	F1	OCA	OOA
MNIST	AIR [18]	0.439±6e-4	0.496±7e-4	0.871±7e-4	0.868±1e-3	N/A	N/A	0.796±5e-3	0.563±4e-3
	N-EM [11]	0.328±4e-3	0.307±6e-3	0.720±1e-3	0.684±2e-3	N/A	N/A	0.000±0e-0	N/A
	IODINE [12]	0.564±1e-3	0.714±1e-3	0.628±2e-3	0.608±3e-3	N/A	N/A	0.286±1e-2	N/A
	GMIOO [21]	<b>0.673±6e-4</b>	<b>0.789±6e-4</b>	<b>0.878±2e-3</b>	<b>0.889±2e-3</b>	<b>0.644±1e-3</b>	<b>0.775±1e-3</b>	<b>0.857±8e-3</b>	<b>0.727±7e-3</b>
	MONet [22]	0.516±2e-4	0.672±2e-4	0.830±5e-4	0.849±4e-4	N/A	N/A	<b>0.912±7e-4</b>	0.481±2e-3
	GENESIS [29]	0.578±5e-4	0.749±3e-4	0.597±2e-3	0.593±2e-3	0.077±3e-4	0.138±4e-4	0.365±6e-3	0.448±5e-3
	SPACE [32]	0.487±1e-3	0.597±2e-3	0.712±8e-4	0.687±7e-4	0.463±5e-4	0.604±5e-4	0.552±3e-3	0.531±1e-2
	Slot Attention [13]	0.561±7e-4	0.736±9e-4	0.528±1e-3	0.418±3e-3	N/A	N/A	0.019±2e-3	N/A
	EfficientMORL [37]	0.093±2e-4	0.002±2e-4	0.535±9e-4	0.465±2e-3	N/A	N/A	0.000±0e-0	N/A
GENESIS-V2 [40]	0.150±8e-5	0.127±2e-4	0.417±2e-4	0.330±2e-4	N/A	N/A	0.019±2e-3	0.498±2e-2	
dSprites	AIR [18]	0.601±3e-4	0.599±4e-4	0.908±5e-4	0.899±7e-4	N/A	N/A	0.732±1e-2	0.726±2e-3
	N-EM [11]	0.559±6e-3	0.592±9e-3	0.754±2e-3	0.642±2e-3	N/A	N/A	0.000±0e-0	N/A
	IODINE [12]	0.850±1e-3	0.930±7e-4	0.834±3e-3	0.875±3e-3	N/A	N/A	0.837±9e-3	N/A
	GMIOO [21]	<b>0.923±6e-4</b>	<b>0.969±3e-4</b>	<b>0.953±1e-3</b>	<b>0.962±2e-3</b>	<b>0.868±1e-3</b>	<b>0.918±1e-3</b>	<b>0.899±4e-3</b>	<b>0.907±1e-2</b>
	MONet [22]	0.798±3e-4	0.900±3e-4	0.907±2e-4	0.925±2e-4	N/A	N/A	0.890±3e-3	0.630±1e-3
	GENESIS [29]	0.818±6e-4	0.918±4e-4	0.761±1e-3	0.798±1e-3	0.078±2e-4	0.141±3e-4	0.502±7e-3	0.427±3e-3
	SPACE [32]	0.865±5e-4	0.941±4e-4	0.869±4e-4	0.860±1e-3	0.745±5e-4	0.827±5e-4	0.492±6e-3	0.569±1e-2
	Slot Attention [13]	0.275±7e-4	0.152±5e-4	0.717±1e-3	0.694±2e-3	N/A	N/A	0.000±0e-0	N/A
	EfficientMORL [37]	0.134±5e-4	0.061±1e-3	0.451±3e-3	0.375±4e-3	N/A	N/A	0.000±1e-3	N/A
GENESIS-V2 [40]	0.545±3e-3	0.583±4e-3	0.858±1e-3	0.868±2e-3	N/A	N/A	0.308±1e-2	0.565±8e-3	
CLEVR	AIR [18]	0.082±3e-4	0.080±2e-4	0.979±4e-4	0.983±5e-4	N/A	N/A	0.924±4e-3	0.920±4e-3
	N-EM [11]	0.095±2e-3	0.130±3e-3	0.105±1e-3	0.055±2e-3	N/A	N/A	0.035±4e-3	N/A
	IODINE [12]	0.540±1e-3	0.536±2e-3	0.970±9e-4	0.973±8e-4	N/A	N/A	0.499±1e-2	N/A
	GMIOO [21]	0.716±6e-4	0.776±7e-4	0.977±5e-4	0.979±9e-4	0.696±2e-3	0.809±2e-3	0.891±3e-3	0.932±4e-3
	MONet [22]	<b>0.882±9e-5</b>	<b>0.934±6e-5</b>	<b>0.985±4e-5</b>	<b>0.989±3e-5</b>	N/A	N/A	<b>0.966±8e-4</b>	0.712±5e-4
	GENESIS [29]	0.391±9e-4	0.502±8e-4	0.263±2e-3	0.218±2e-3	0.117±5e-4	0.174±4e-4	0.143±5e-3	0.737±1e-2
	SPACE [32]	0.795±3e-4	0.859±3e-4	0.972±1e-4	0.975±3e-4	<b>0.775±7e-4</b>	<b>0.862±7e-4</b>	0.710±2e-3	<b>0.936±7e-3</b>
	Slot Attention [13]	0.240±3e-4	0.026±2e-4	0.982±3e-4	0.984±6e-4	N/A	N/A	0.002±1e-3	N/A
	EfficientMORL [37]	0.565±2e-3	0.616±3e-3	0.826±4e-3	0.779±6e-3	N/A	N/A	0.284±1e-2	N/A
GENESIS-V2 [40]	0.190±6e-4	0.023±8e-4	0.639±2e-3	0.585±2e-3	N/A	N/A	0.206±8e-3	0.712±2e-2	
SHOP	AIR [18]	0.511±2e-4	0.467±3e-4	0.896±3e-4	0.904±4e-4	N/A	N/A	0.308±1e-2	0.672±2e-3
	N-EM [11]	0.116±9e-4	0.184±2e-3	0.145±7e-4	0.082±1e-3	N/A	N/A	0.009±3e-3	N/A
	IODINE [12]	0.714±1e-3	0.723±3e-3	0.837±1e-3	0.795±2e-3	N/A	N/A	0.344±6e-3	N/A
	GMIOO [21]	0.776±2e-4	0.829±2e-4	0.958±2e-4	0.962±4e-4	<b>0.754±6e-4</b>	<b>0.843±7e-4</b>	0.669±5e-3	<b>0.940±6e-3</b>
	MONet [22]	<b>0.784±2e-4</b>	<b>0.854±3e-4</b>	0.941±1e-4	0.946±2e-4	N/A	N/A	<b>0.861±2e-3</b>	<b>0.881±2e-3</b>
	GENESIS [29]	0.316±3e-4	0.102±2e-4	0.265±2e-4	0.158±5e-4	0.169±5e-4	0.250±7e-4	0.000±0e-0	0.749±8e-3
	SPACE [32]	0.757±3e-4	0.827±3e-4	0.902±5e-4	0.897±6e-4	0.742±4e-4	0.840±4e-4	0.297±2e-3	0.759±4e-3
	Slot Attention [13]	0.388±6e-4	0.159±1e-3	0.962±3e-4	0.969±4e-4	N/A	N/A	0.000±5e-4	N/A
	EfficientMORL [37]	0.502±1e-3	0.319±3e-3	<b>0.964±7e-4</b>	<b>0.973±1e-3</b>	N/A	N/A	0.040±3e-3	N/A
GENESIS-V2 [40]	0.314±3e-4	0.067±3e-4	0.930±9e-4	0.937±9e-4	N/A	N/A	0.001±6e-4	0.641±2e-2	

representations with implicit 3D representations to better model and learn from 3D visual scenes, and with embodied perception to autonomously obtain more information from visual scenes and thus learn better representations. The other aspect is the application of compositional scene representations. For example, accumulating knowledge of visual scenes by continually learning more and more visual concepts based on compositional scene representations, which in turn helps the understanding of visual scenes.

### 6.1 Learning with Implicit 3D Modeling

With the introduction of NeRF [69], implicit 3D representations which describe 3D models with implicit functions have recently received more and more attention. Compared with explicit 3D representations such as mesh, point cloud, and voxel, implicit 3D representations have better differentiable properties, and can be used to render images with arbitrary resolution. Compared with directly transforming

scene representations into 2D appearances and shapes, implicit 3D representations have the advantage of maintaining constancy among different viewpoints. A series of improvements and extensions of NeRF, such as NeRF-- [70], KiloNeRF [71], GRF [72], and NeRF-VAE [73], lay the foundation for the combination of compositional scene representations and implicit 3D representations. ObSuRF [74] and uORF [75] have made preliminary explorations in this promising direction, and more researches are expected.

### 6.2 Learning with Embodied Agents

Compared to passively learning compositional scene representations only from observational data, autonomously interacting with and purposefully changing the environment via embodied agents [76] can acquire more information from visual scenes, which in turn results in more efficient learning. Learning compositional scene representations with embodied agents can make better use of the interactivity of

TABLE 4  
Comparison of different compositional scene representation learning methods on the Test 2 splits.

Dataset	Method	AMI-A	ARI-A	AMI-O	ARI-O	IoU	F1	OCA	OOA
MNIST	AIR [18]	0.526±3e-4	0.572±6e-4	0.827±8e-4	0.781±1e-3	N/A	N/A	0.526±8e-3	0.537±4e-3
	N-EM [11]	0.317±2e-3	0.271±3e-3	0.553±2e-3	0.457±2e-3	N/A	N/A	0.006±2e-3	N/A
	IODINE [12]	0.518±2e-3	0.633±2e-3	0.650±2e-3	0.562±4e-3	N/A	N/A	0.365±9e-3	N/A
	GMIOO [21]	<b>0.661±5e-4</b>	<b>0.761±5e-4</b>	<b>0.851±3e-4</b>	<b>0.833±2e-4</b>	<b>0.607±8e-4</b>	<b>0.739±8e-4</b>	<b>0.686±7e-3</b>	<b>0.701±5e-3</b>
	MONet [22]	0.451±2e-4	0.575±2e-4	0.785±2e-4	0.755±2e-4	N/A	N/A	0.535±2e-3	0.473±1e-3
	GENESIS [29]	0.458±4e-4	0.628±3e-4	0.536±8e-4	0.431±1e-3	0.076±1e-4	0.135±2e-4	0.298±8e-3	0.464±3e-3
	SPACE [32]	0.429±1e-3	0.519±1e-3	0.684±1e-3	0.599±1e-3	0.374±3e-4	0.505±3e-4	0.311±7e-3	0.551±9e-3
	Slot Attention [13]	0.493±1e-3	0.630±1e-3	0.605±1e-3	0.467±2e-3	N/A	N/A	0.039±4e-3	N/A
	EfficientMORL [37]	0.156±3e-4	0.011±2e-4	0.551±7e-4	0.423±1e-3	N/A	N/A	0.001±1e-3	N/A
GENESIS-V2 [40]	0.205±1e-4	0.122±5e-5	0.509±2e-4	0.393±3e-4	N/A	N/A	0.210±1e-2	0.529±9e-3	
dSprites	AIR [18]	0.758±3e-4	0.746±4e-4	0.880±3e-4	0.832±4e-4	N/A	N/A	0.358±6e-3	0.726±2e-3
	N-EM [11]	0.558±1e-3	0.488±3e-3	0.749±1e-3	0.629±2e-3	N/A	N/A	0.027±3e-3	N/A
	IODINE [12]	0.821±3e-4	0.906±4e-4	0.840±3e-4	0.853±6e-4	N/A	N/A	0.602±7e-3	N/A
	GMIOO [21]	<b>0.903±5e-4</b>	<b>0.958±3e-4</b>	<b>0.931±6e-4</b>	<b>0.929±1e-3</b>	<b>0.794±2e-3</b>	<b>0.857±2e-3</b>	<b>0.632±9e-3</b>	<b>0.879±3e-3</b>
	MONet [22]	0.776±2e-4	0.883±2e-4	0.867±3e-4	0.858±3e-4	N/A	N/A	0.592±5e-3	0.674±3e-4
	GENESIS [29]	0.748±5e-4	0.881±4e-4	0.712±6e-4	0.680±1e-3	0.067±2e-4	0.121±3e-4	0.290±8e-3	0.420±2e-3
	SPACE [32]	0.813±5e-4	0.906±6e-4	0.835±7e-4	0.798±1e-3	0.599±9e-4	0.694±8e-4	0.289±8e-3	0.619±7e-3
	Slot Attention [13]	0.362±4e-4	0.196±2e-4	0.749±6e-4	0.705±9e-4	N/A	N/A	0.000±8e-4	N/A
	EfficientMORL [37]	0.197±5e-4	0.059±9e-4	0.488±1e-3	0.353±2e-3	N/A	N/A	0.011±2e-3	N/A
GENESIS-V2 [40]	0.616±2e-3	0.646±3e-3	0.826±6e-4	0.800±9e-4	N/A	N/A	0.295±2e-2	0.580±3e-3	
CLEVR	AIR [18]	0.044±1e-4	0.034±1e-4	0.954±4e-4	0.952±8e-4	N/A	N/A	<b>0.645±5e-3</b>	0.880±1e-3
	N-EM [11]	0.128±4e-4	0.178±7e-4	0.143±7e-4	0.063±6e-4	N/A	N/A	0.013±3e-3	N/A
	IODINE [12]	0.576±3e-4	0.478±1e-3	0.954±1e-3	0.952±2e-3	N/A	N/A	0.339±1e-2	N/A
	GMIOO [21]	0.727±3e-4	0.741±5e-4	0.956±3e-4	0.949±5e-4	0.649±1e-3	0.757±9e-4	0.525±6e-3	<b>0.907±3e-3</b>
	MONet [22]	<b>0.850±3e-4</b>	<b>0.896±8e-4</b>	<b>0.957±3e-4</b>	<b>0.955±3e-4</b>	N/A	N/A	0.596±4e-3	0.737±4e-4
	GENESIS [29]	0.324±6e-4	0.411±6e-4	0.230±2e-3	0.150±2e-3	0.063±1e-4	0.106±1e-4	0.221±1e-2	0.577±5e-3
	SPACE [32]	0.781±2e-4	0.822±3e-4	0.939±4e-4	0.931±5e-4	<b>0.683±4e-4</b>	<b>0.773±5e-4</b>	0.416±3e-3	0.894±4e-3
	Slot Attention [13]	0.378±2e-4	0.078±8e-5	0.945±5e-4	0.939±8e-4	N/A	N/A	0.011±2e-3	N/A
	EfficientMORL [37]	0.535±1e-3	0.494±3e-3	0.776±2e-3	0.696±3e-3	N/A	N/A	0.054±5e-3	N/A
GENESIS-V2 [40]	0.289±1e-3	0.066±1e-3	0.665±2e-3	0.551±2e-3	N/A	N/A	0.218±7e-3	0.730±8e-3	
SHOP	AIR [18]	0.636±1e-4	0.563±3e-4	0.857±1e-4	0.831±4e-4	N/A	N/A	0.264±1e-2	0.650±1e-3
	N-EM [11]	0.234±1e-3	0.302±3e-3	0.273±8e-4	0.160±1e-3	N/A	N/A	0.002±1e-3	N/A
	IODINE [12]	0.703±2e-3	0.638±6e-3	0.846±9e-4	0.789±7e-4	N/A	N/A	0.263±8e-3	N/A
	GMIOO [21]	<b>0.759±3e-4</b>	0.773±2e-4	0.926±3e-4	0.917±9e-4	0.652±1e-3	0.743±1e-3	0.341±8e-3	<b>0.876±1e-3</b>
	MONet [22]	0.752±1e-4	<b>0.796±2e-4</b>	0.900±1e-4	0.885±2e-4	N/A	N/A	<b>0.375±2e-3</b>	0.809±1e-3
	GENESIS [29]	0.326±2e-4	0.087±2e-4	0.360±4e-4	0.188±3e-4	0.105±1e-4	0.171±2e-4	0.000±0e-0	0.681±3e-3
	SPACE [32]	0.736±2e-4	0.771±2e-4	0.874±4e-4	0.857±9e-4	<b>0.663±6e-4</b>	<b>0.767±7e-4</b>	0.269±6e-3	0.669±9e-3
	Slot Attention [13]	0.487±1e-3	0.194±3e-3	<b>0.942±6e-4</b>	<b>0.950±4e-4</b>	N/A	N/A	0.000±0e-0	N/A
	EfficientMORL [37]	0.545±6e-4	0.292±1e-3	0.934±8e-4	0.941±1e-3	N/A	N/A	0.042±5e-3	N/A
GENESIS-V2 [40]	0.426±3e-4	0.119±6e-4	0.900±9e-4	0.903±1e-3	N/A	N/A	0.003±1e-3	0.613±1e-2	

the physical world, and thus are more likely to be applicable to complex visual scenes under the restriction that no object-level supervision is available. Some methods, such as COBRA [77] and Grasp2Vec [78], have made preliminary explorations in this direction. Future work in this direction may include imitating the development of human infants by combining compositional scene representations with embodied perception to simultaneously learn visual perception and motor skills in real indoor environments.

### 6.3 Continual Learning of Visual Concepts

In reality, the variety of visual concepts is extremely rich, and visual concepts appearing in visual scenes are ever-changing. In order to learn effectively in this scenario, it is important for compositional scene representation methods to be able to continually learn visual concepts from new data. Besides the problem of catastrophic forgetting, learning compositional scene representations in the continual

setting also faces the challenges like identifying previously seen visual concepts and learning new visual concepts in the presence of object occlusions. ADI [79] adopts a two-stage learning strategy, and has made preliminary explorations in the acquisition and utilization of knowledge, which is an important ingredient in this research direction. Future work may include continually acquiring and utilizing knowledge of visual concepts without explicit learning stages, and continually grouping visual concepts into non-semantic categories based on occlusion-aware online clustering.

## 7 CONCLUSIONS

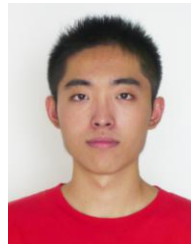
The research on reconstruction-based compositional scene representation learning has only emerged in the last few years, and has gradually gained more attention due to its research significance. This survey has introduced the problem setting and development history of this research problem, and categorized existing methods in terms of

modeling of visual scenes and inference of scene representations. Representative methods that consider the most extensively studied problem setting and form the foundation for other methods have been benchmarked on four datasets, and an open source toolbox that includes the code for creating datasets and evaluating the performance of the chosen methods has been provided to reproduce the benchmark experiments. This research topic has broad research prospects, and future directions include learning with implicit 3D modeling, learning with embodied agents, and continual learning of visual concepts. It is believed that this research topic will continue to gain more attentions in the coming years, and continuous research progresses in this topic will promote the development of more human-like artificial intelligence systems.

## REFERENCES

- [1] D. Cireřan, U. Meier, J. Masci, and J. Schmidhuber, "A committee of neural networks for traffic sign classification," in *IJCNN*, 2011, pp. 1918–1921.
- [2] A. Krizhevsky, I. Sutskever, and G. E. Hinton, "Imagenet classification with deep convolutional neural networks," in *NeurIPS*, vol. 25, 2012.
- [3] K. He, X. Zhang, S. Ren, and J. Sun, "Deep residual learning for image recognition," in *CVPR*, 2016, pp. 770–778.
- [4] S. Grossberg, E. Mingolla, and W. D. Ross, "Visual brain and visual perception: How does the cortex do perceptual grouping?" *Trends in Neurosciences*, vol. 20, no. 3, pp. 106–111, 1997.
- [5] A. Treisman, "The binding problem," *Current Opinion in Neurobiology*, vol. 6, no. 2, pp. 171–178, 1996.
- [6] J. M. Wolfe and K. R. Cave, "The psychophysical evidence for a binding problem in human vision," *Neuron*, vol. 24, no. 1, pp. 11–17, 1999.
- [7] K. Koffka, *Principles of Gestalt Psychology*. US: Harbrace J, 1935.
- [8] P. M. Milner, "A model for visual shape recognition." *Psychological Review*, vol. 81, no. 6, pp. 521–535, 1974.
- [9] A. M. Treisman and G. Gelade, "A feature-integration theory of attention," *Cognitive Psychology*, vol. 12, no. 1, pp. 97–136, 1980.
- [10] K. Greff, R. K. Srivastava, and J. Schmidhuber, "Binding via reconstruction clustering," in *ICLR Workshop*, 2016.
- [11] K. Greff, S. van Steenkiste, and J. Schmidhuber, "Neural expectation maximization," in *NeurIPS*, vol. 30, 2017.
- [12] K. Greff, R. L. Kaufman, R. Kabra, N. Watters, C. Burgess, D. Zoran, L. Matthey, M. Botvinick, and A. Lerchner, "Multi-object representation learning with iterative variational inference," in *ICML*, vol. 97, 06 2019, pp. 2424–2433.
- [13] F. Locatello, D. Weissenborn, T. Unterthiner, A. Mahendran, G. Heigold, J. Uszkoreit, A. Dosovitskiy, and T. Kipf, "Object-centric learning with slot attention," in *NeurIPS*, vol. 33, 2020, pp. 11 525–11 538.
- [14] K. Greff, A. Rasmus, M. Berglund, T. Hao, H. Valpola, and J. Schmidhuber, "Tagger: Deep unsupervised perceptual grouping," in *NeurIPS*, vol. 29, 2016.
- [15] I. Prémont-Schwarz, A. Ilin, T. Hao, A. Rasmus, R. Boney, and H. Valpola, "Recurrent ladder networks," in *NeurIPS*, vol. 30, 2017.
- [16] S. van Steenkiste, M. Chang, K. Greff, and J. Schmidhuber, "Relational neural expectation maximization: Unsupervised discovery of objects and their interactions," in *ICLR*, 2018.
- [17] J. Huang and K. Murphy, "Efficient inference in occlusion-aware generative models of images," in *ICLR Workshop*, 2016.
- [18] S. M. A. Eslami, N. Heess, T. Weber, Y. Tassa, D. Szepesvari, K. Kavukcuoglu, and G. E. Hinton, "Attend, infer, repeat: Fast scene understanding with generative models," in *NeurIPS*, vol. 29, 2016.
- [19] J. Yuan, B. Li, and X. Xue, "Spatial mixture models with learnable deep priors for perceptual grouping," in *AAAI*, vol. 33, no. 01, 07 2019, pp. 9135–9142.
- [20] A. Kosiorek, H. Kim, Y. W. Teh, and I. Posner, "Sequential attend, infer, repeat: Generative modelling of moving objects," in *NeurIPS*, vol. 31, 2018.
- [21] J. Yuan, B. Li, and X. Xue, "Generative modeling of infinite occluded objects for compositional scene representation," in *ICML*, vol. 97, 06 2019, pp. 7222–7231.
- [22] C. P. Burgess, L. Matthey, N. Watters, R. Kabra, I. Higgins, M. Botvinick, and A. Lerchner, "Monet: Unsupervised scene decomposition and representation," *arXiv:1901.11390*, 01 2019.
- [23] K. Stelzner, R. Peharz, and K. Kersting, "Faster attend-infer-repeat with tractable probabilistic models," in *ICML*, vol. 97, 06 2019, pp. 5966–5975.
- [24] T. Xu, C. Li, J. Zhu, and B. Zhang, "Multi-objects generation with amortized structural regularization," in *NeurIPS*, vol. 32, 2019.
- [25] E. Crawford and J. Pineau, "Spatially invariant unsupervised object detection with convolutional neural networks," in *AAAI*, vol. 33, no. 01, 07 2019, pp. 3412–3420.
- [26] A. Stanić and J. Schmidhuber, "R-sqair: Relational sequential attend, infer, repeat," in *NeurIPS Workshop*, 2019.
- [27] N. Li, C. Eastwood, and R. Fisher, "Learning object-centric representations of multi-object scenes from multiple views," in *NeurIPS*, vol. 33, 2020, pp. 5656–5666.
- [28] Y. Yang, Y. Chen, and S. Soatto, "Learning to manipulate individual objects in an image," in *CVPR*, 2020, pp. 6557–6566.
- [29] M. Engelcke, A. R. Kosiorek, O. P. Jones, and I. Posner, "Genesis: Generative scene inference and sampling with object-centric latent representations," in *ICLR*, 2020.
- [30] J. Jiang and S. Ahn, "Generative neurosymbolic machines," in *NeurIPS*, vol. 33, 2020, pp. 12 572–12 582.
- [31] J. Jiang, S. Janghorbani, G. de Melo, and S. Ahn, "Scalor: Generative world models with scalable object representations," in *ICLR*, 2020.
- [32] Z. Lin, Y.-F. Wu, S. V. Peri, W. Sun, G. Singh, F. Deng, J. Jiang, and S. Ahn, "Space: Unsupervised object-oriented scene representation via spatial attention and decomposition," in *ICLR*, 2020.
- [33] Z. Lin, Y.-F. Wu, S. Peri, B. Fu, J. Jiang, and S. Ahn, "Improving generative imagination in object-centric world models," in *ICML*, vol. 119, 07 2020, pp. 6140–6149.
- [34] E. Crawford and J. Pineau, "Exploiting spatial invariance for scalable unsupervised object tracking," in *AAAI*, vol. 34, no. 04, 04 2020, pp. 3684–3692.
- [35] L. Nanbo, M. A. Raza, H. Wenbin, Z. Sun, and R. B. Fisher, "Object-centric representation learning with generative spatial-temporal factorization," in *NeurIPS*, 2021.
- [36] P. Zablotzkaia, E. A. Dominici, L. Sigal, and A. M. Lehrmann, "Provide: A probabilistic framework for unsupervised video decomposition," in *UAI*, vol. 161, 07 2021, pp. 2019–2028.
- [37] P. Emami, P. He, S. Ranka, and A. Rangarajan, "Efficient iterative amortized inference for learning symmetric and disentangled multi-object representations," in *ICML*, vol. 139, 07 2021, pp. 2970–2981.
- [38] R. Kabra, D. Zoran, G. Erdogan, L. Matthey, A. Creswell, M. Botvinick, A. Lerchner, and C. P. Burgess, "Simone: View-invariant, temporally-abstracted object representations via unsupervised video decomposition," in *NeurIPS*, 2021.
- [39] J. Yuan, B. Li, and X. Xue, "Unsupervised learning of compositional scene representations from multiple unspecified viewpoints," in *AAAI*, 2022.
- [40] M. Engelcke, O. P. Jones, and I. Posner, "Genesis-v2: Inferring unordered object representations without iterative refinement," in *NeurIPS*, 2021.
- [41] M. A. Weis, K. Chitta, Y. Sharma, W. Brendel, M. Bethge, A. Geiger, and A. S. Ecker, "Benchmarking unsupervised object representations for video sequences," *Journal of Machine Learning Research*, vol. 22, no. 183, pp. 1–61, 2021.
- [42] F. Deng, Z. Zhi, D. Lee, and S. Ahn, "Generative scene graph networks," in *ICLR*, 2021.
- [43] C. Chen, F. Deng, and S. Ahn, "Roots: Object-centric representation and rendering of 3d scenes," *Journal of Machine Learning Research*, vol. 22, no. 259, pp. 1–36, 2021.
- [44] J. Gilmer, S. S. Schoenholz, P. F. Riley, O. Vinyals, and G. E. Dahl, "Neural message passing for quantum chemistry," in *ICML*, vol. 70, 08 2017, pp. 1263–1272.
- [45] Y. Duan, M. Andrychowicz, B. Stadie, O. Jonathan Ho, J. Schneider, I. Sutskever, P. Abbeel, and W. Zaremba, "One-shot imitation learning," in *NeurIPS*, vol. 30, 2017.
- [46] J. Redmon, S. Divvala, R. Girshick, and A. Farhadi, "You only look once: Unified, real-time object detection," in *CVPR*, 2016, pp. 779–788.

- [47] A. Santoro, R. Faulkner, D. Raposo, J. Rae, M. Chrzanowski, T. Weber, D. Wierstra, O. Vinyals, R. Pascanu, and T. Lillicrap, "Relational recurrent neural networks," in *NeurIPS*, vol. 31, 2018.
- [48] D. Bear, C. Fan, D. Mrowca, Y. Li, S. Alter, A. Nayebi, J. Schwartz, L. F. Fei-Fei, J. Wu, J. Tenenbaum, and D. L. Yamins, "Learning physical graph representations from visual scenes," in *NeurIPS*, vol. 33, 2020, pp. 6027–6039.
- [49] Z. He, J. Li, D. Liu, H. He, and D. Barber, "Tracking by animation: Unsupervised learning of multi-object attentive trackers," in *CVPR*, 2019, pp. 1318–1327.
- [50] Y. Du, K. Smith, T. Ullman, J. Tenenbaum, and J. Wu, "Unsupervised discovery of 3d physical objects from video," in *ICLR*, 2021.
- [51] T. Monnier, E. Vincent, J. Ponce, and M. Aubry, "Unsupervised layered image decomposition into object prototypes," in *ICCV*, 2021, pp. 8640–8650.
- [52] A. Villar-Corrales and S. Behnke, "Unsupervised image decomposition with phase-correlation networks," in *VISAPP*, 2022.
- [53] D. Smirnov, M. Gharbi, M. Fisher, V. Guizilini, A. Efros, and J. M. Solomon, "Marionette: Self-supervised sprite learning," *NeurIPS*, vol. 34, 2021.
- [54] Y. W. Teh, D. Grür, and Z. Ghahramani, "Stick-breaking construction for the indian buffet process," in *AISTATS*, vol. 2, 03 2007, pp. 556–563.
- [55] J. von Kügelgen, I. Ustyuzhaninov, P. Gehler, M. Bethge, and B. Schölkopf, "Towards causal generative scene models via competition of experts," in *ICLR Workshop*, 2020.
- [56] A. P. Dempster, N. M. Laird, and D. B. Rubin, "Maximum likelihood from incomplete data via the em algorithm," *Journal of the Royal Statistical Society: Series B (Methodological)*, vol. 39, no. 1, pp. 1–22, 1977.
- [57] Z. Ghahramani and T. Griffiths, "Infinite latent feature models and the indian buffet process," in *NeurIPS*, vol. 18, 2006.
- [58] T. L. Griffiths and Z. Ghahramani, "The indian buffet process: An introduction and review," *Journal of Machine Learning Research*, vol. 12, no. 32, pp. 1185–1224, 2011.
- [59] J. Marino, Y. Yue, and S. Mandt, "Iterative amortized inference," in *ICML*, vol. 80, 07 2018, pp. 3403–3412.
- [60] D. J. Rezende and F. Viola, "Taming vaes," *arXiv:1810.00597*, 2018.
- [61] O. Ronneberger, P. Fischer, and T. Brox, "U-net: Convolutional networks for biomedical image segmentation," in *MICCAI*, 2015, pp. 234–241.
- [62] Y. LeCun, C. Cortes, and C. Burges, "The mnist dataset of handwritten digits (images)," *NYU: New York, NY, USA*, 1999.
- [63] L. Matthey, I. Higgins, D. Hassabis, and A. Lerchner, "dsprites: Disentanglement testing sprites dataset," <https://github.com/deepmind/dsprites-dataset/>, 2017.
- [64] J. Johnson, B. Hariharan, L. van der Maaten, L. Fei-Fei, C. L. Zitnick, and R. Girshick, "Clevr: A diagnostic dataset for compositional language and elementary visual reasoning," in *CVPR*, 2017, pp. 1988–1997.
- [65] M. Nazarczuk and K. Mikolajczyk, "Shop-vrb: A visual reasoning benchmark for object perception," in *ICRA*, 2020, pp. 6898–6904.
- [66] R. Kabra, C. Burgess, L. Matthey, R. L. Kaufman, K. Greff, M. Reynolds, and A. Lerchner, "Multi-object datasets," <https://github.com/deepmind/multi-object-datasets/>, 2019.
- [67] N. X. Vinh, J. Epps, and J. Bailey, "Information theoretic measures for clusterings comparison: Variants, properties, normalization and correction for chance," *Journal of Machine Learning Research*, vol. 11, no. 95, pp. 2837–2854, 2010.
- [68] L. Hubert and P. Arabie, "Comparing partitions," *Journal of Classification*, vol. 2, no. 1, pp. 193–218, 12 1985.
- [69] B. Mildenhall, P. P. Srinivasan, M. Tancik, J. T. Barron, R. Ramamoorthi, and R. Ng, "Nerf: Representing scenes as neural radiance fields for view synthesis," in *ECCV*, 2020, pp. 405–421.
- [70] Z. Wang, S. Wu, W. Xie, M. Chen, and V. A. Prisacariu, "Nerf-: Neural radiance fields without known camera parameters," *arXiv:2102.07064*, 02 2021.
- [71] C. Reiser, S. Peng, Y. Liao, and A. Geiger, "Kilonerf: Speeding up neural radiance fields with thousands of tiny mlps," in *ICCV*, 2021, pp. 14 335–14 345.
- [72] A. Trevithick and B. Yang, "Grf: Learning a general radiance field for 3d representation and rendering," in *ICCV*, 2021, pp. 15 182–15 192.
- [73] A. R. Kosiorek, H. Strathmann, D. Zoran, P. Moreno, R. Schneider, S. Mokra, and D. J. Rezende, "Nerf-vae: A geometry aware 3d scene generative model," in *ICML*, vol. 139, 07 2021, pp. 5742–5752.
- [74] K. Stelzner, K. Kersting, and A. R. Kosiorek, "Decomposing 3d scenes into objects via unsupervised volume segmentation," *arXiv:2104.01148*, 04 2021.
- [75] H.-X. Yu, L. J. Guibas, and J. Wu, "Unsupervised discovery of object radiance fields," *arXiv:2107.07905*, 07 2021.
- [76] A. T. Taylor, T. A. Berrueta, and T. D. Murphey, "Active learning in robotics: A review of control principles," *Mechatronics*, vol. 77, p. 102576, 2021.
- [77] N. Watters, L. Matthey, M. Bosnjak, C. P. Burgess, and A. Lerchner, "Cobra: Data-efficient model-based rl through unsupervised object discovery and curiosity-driven exploration," *arXiv:1905.09275*, 05 2019.
- [78] E. Jang, C. Devin, V. Vanhoucke, and S. Levine, "Grasp2vec: Learning object representations from self-supervised grasping," in *CoRL*, vol. 87, 10 2018, pp. 99–112.
- [79] J. Yuan, B. Li, and X. Xue, "Knowledge-guided object discovery with acquired deep impressions," in *AAAI*, vol. 35, no. 12, 05 2021, pp. 10 798–10 806.



**Jinyang Yuan** received the BS degree in physics from Nanjing University, China, and the MS degree in electrical engineering from University of California, San Diego. He is currently a PhD candidate in the School of Computer Science, Fudan University, China. His research interests include computer vision, machine learning, and deep generative models.



**Tonglin Chen** is currently pursuing the PhD degree in computer science from Fudan University, Shanghai, China. His current research interests include machine learning, deep generative models, and object-centric representation learning.



**Bin Li** received the PhD degree in computer science from Fudan University, Shanghai, China. He is an associate professor with the School of Computer Science, Fudan University, Shanghai, China. Before joining Fudan University, Shanghai, China, he was a lecturer with the University of Technology Sydney, Australia and a senior research scientist with Data61 (formerly NICTA), CSIRO, Australia. His current research interests include machine learning and visual intelligence, particularly in compositional scene representation, modeling and inference.



**Xiangyang Xue** received the BS, MS, and PhD degrees in communication engineering from Xi-dian University, Xian, China, in 1989, 1992, and 1995, respectively. He is currently a professor of computer science with Fudan University, Shanghai, China. His research interests include multimedia information processing and machine learning.